

# Time series forecasting based on optimized LLM for fault prediction in distribution power grid insulators

João P. Matos-Carvalho<sup>a,b,c</sup>, Stefano Frizzo Stefenon<sup>d</sup>, Valderi Reis Quietinho Leithardt<sup>e</sup>, Kin-Choong Yow<sup>d</sup>

<sup>a</sup>*LASIGE, Departamento de Informática, Faculdade de Ciências, Universidade de Lisboa, 1749-016 Lisboa, Portugal,*

<sup>b</sup>*Center of Technology and Systems (UNINOVA-CTS) and Associated Lab of Intelligent Systems (LASI), Caparica, 2829-516, Portugal*

<sup>c</sup>*COPELABS, Lusófona University, Campo Grande, 376, Lisboa, 1749-024, Portugal*

<sup>d</sup>*Faculty of Engineering and Applied Sciences, University of Regina, Saskatchewan, S4S 0A2, Canada*

<sup>e</sup>*Instituto Universitário de Lisboa (ISCTE-IUL), ISTAR, Lisboa, Portugal*

---

## Abstract

Surface contamination on electrical grid insulators leads to an increase in leakage current until an electrical discharge occurs, which can result in a power system shutdown. To mitigate the possibility of disruptive faults resulting in a power outage, monitoring contamination and leakage current can help predict the progression of faults. Given this need, this paper proposes a hybrid deep learning (DL) model for predicting the increase in leakage current in high-voltage insulators. The hybrid structure considers a multi-criteria optimization using tree-structured Parzen estimation, an input stage filter for signal noise attenuation combined with a large language model (LLM) applied for time series forecasting. The proposed optimized LLM outperforms state-of-the-art DL models with a root-mean-square error equal to  $2.24 \times 10^{-4}$  for a short-term horizon and  $1.21 \times 10^{-3}$  for a medium-term horizon.

*Keywords:*

Deep learning, LLM; multi-criteria optimization, power grid insulator, time series forecasting

---

## 1. Introduction

Insulators in the conventional electrical power distribution and transmission system are installed outdoors and are susceptible to environmental conditions such as the presence of contamination, solar radiation, atmospheric discharges, and thermal variation [1]. These environmental stresses can result in a power outage if preventive or predictive maintenance is not handled [2].

A way of identifying where the power grid needs more attention is to perform inspections on the electrical system, either through imaging or using specific equipment to assess the condition of the system [3]. Besides monitoring using specific equipment such as ultrasound, radio interference, ultraviolet, and infrared cameras, an analysis can be done in terms of power grid contamination. The contamination of insulators is a subject that has been extensively studied, because over time the contamination increases the surface conductivity of the insulators, resulting in flashover [4].

Specific techniques for measuring the contamination of insulators, whether this is saline contamination or based on kaolin (artificial contamination) are explored. Measuring leakage current is one way of determining how the contamination is influencing the insulator's degradation [5]. The higher the surface conductivity of the insulator, the greater the chance of this

component experiencing leakage current, which leads to a flashover voltage in the power system that can result in a complete shutdown of the grid [6].

Considering the advances made in predicting time series using machine learning (ML)-based models, especially involving deep learning (DL) [7], using them to predict the increase in leakage current could be an alternative for improving the monitoring performance of electrical systems. Based on this premise, this paper proposes a hybrid model for predicting leakage current in electric power distribution insulators. Given the vast nomenclature of the field, the acronyms of this paper are standardized according to Table 1.

The proposed hybrid model employs noise attenuation considering an input filter stage. The Christiano Fitzgerald (CF) asymmetric random walk [8], Hodrick-Prescott (HP) [9], season-trend decomposition using LOESS (STL) [10], multiple STL (MSTL) [11], empirical wavelet transform (EWT) [12], Butterworth [13], and empirical mode decomposition (EDM) [14] filters are analyzed, and the best filter is employed in the model input. For the STL and MSTL, the LOESS stands for locally estimated scatterplot smoothing.

Based on the filtered signal, the LLM is used to perform the time series prediction, also known as timeLLM. To ensure that the best structure is used, the Optuna framework using the tree-structured Parzen estimator (TPE) is considered for hyperparameter tuning [15]. Considering the proposed optimized LLM model applied for fault prediction, this paper has the following contributions:

- It presents an innovative way of analyzing time series based on LLM models, and is a strategy that can be applied in the future considering the advances in this field.
- By using a filter on the input signal, unrepresentative noises are disregarded, making the prediction model more assertive and promising in chaotic time series analysis.
- Based on a strategy using TPE, the structure is hyper-adjusted ensuring that the optimal hyperparameters are used in the proposed model.

The remainder of this paper is as follows: In section 2, related works about fault prediction in insulators are presented. Section 3 explains the proposed optimized LLM model. In section 4 the results of the application of the proposed model are discussed, firstly the evaluation of the filter is presented, followed by the tuning strategy. Considering a hypertuned structure, a statistical analysis and benchmarking are presented. Section 5 presents final remarks and directions for future research.

## 2. Related Works

Fault prediction in distribution grid insulators is critical for maintaining the reliability and safety of power systems [16]. Recent studies have explored various methodologies to predict insulator failures, focusing on analyzing leakage currents, employing ML techniques, and utilizing advanced signal processing methods. A way to identify faults in this context involves monitoring the time series data of the leakage current of insulators under contaminated conditions.

Several authors have applied computer vision-based methods considering convolutional neural networks (CNNs) for insulator fault identification [17]. Prominent in this area is the you only look once (YOLO) model, which was applied in its third generation by Yang et al. [18], in the fourth generation by Li et al. [19], in the fifth generation by Zhou et al. [20], considering a hypertuned version by Stefenon et al. [21], or using a hybrid version in [22].

Deng et al. [23] proposed a modified YOLO that can be computed on edge devices. The modification to make the algorithm more efficient was in the backbone of the YOLO. Instead of using a CSPDarknet53 (standard for the YOLO version that they considered), they applied a

Table 1: Acronyms considered in this paper.

Acronym	Name
ANFIS	Adaptive neuro-fuzzy inference system
AR	Auto-regressive
A-LSTM	Attention-based long short-term memory
CF	Christiano Fitzgerald
CNN	Convolutional neural networks
DL	Deep learning
DeepNPTS	Deep non-parametric time series
DeepTCN	Deep temporal convolutional network
EI	Expected improvement
EMD	Empirical mode decomposition
EWT	Empirical wavelet transform
GMDH	Group method of data handling
GRU	Gated recurrent unit
HP	Hodrick-Prescott
HFCM	High order fuzzy cognitive maps
IMF	Intrinsic mode function
KDE	Kernel density estimation
LLM	Large language model
LOESS	Locally estimated scatterplot smoothing
LSTM	Long short-term memory
MAE	Mean absolute error
MAPE	Mean absolute percentage error
ML	Machine learning
MSTL	Multiple season-trend decomposition using LOESS
N-BEATS	Neural basis expansion analysis
NHINTS	Neural hierarchical interpolation for time series
RMSE	Root-mean-square error
RNN	Recurrent neural network
SMAPE	Symmetric mean absolute percentage error
STGCN	Spatiotemporal graph convolutional network
STL	Season-trend decomposition using LOESS
SVM	Support vector machine
TCN	Temporal convolutional networks
TFT	Temporal fusion transformer
Time-LLM	Time large language model
TPE	Tree-structured Parzen estimator
YOLO	You only look once

lightweight network MobilieNetv3. Based on this modification, the proposed algorithm achieved an accuracy of 0.945 with a speed of 58.5 frames per second. He et al. [24] also applied a modified version of YOLO, considering a model called multi-fault insulator detection they achieved an accuracy of 0.939.

Zhao et al. [25] presented an improved faster region CNN for insulator fault detection. They considered preprocessing techniques for image segmentation, reducing the image noise, and having the focus on the insulators, even when complex backgrounds are considered. Based on their model, it was possible to achieve a mean average precision of 0.908 considering glass insulators and 0.917 when composite insulators were evaluated. Based on CNNs, Lin et al. [26] considered infrared images for insulator defect diagnosis. Applications based on CNNs are promising, as they can be handled indirectly (without contact with the electrical network) [27], while in the case of leakage current it is necessary to measure the insulators directly, making it a more challenging approach.

Sopelsa Neto et al. [28] subjected insulators to saline environments to simulate contamination and analyzed the progression of leakage currents leading up to disruptive discharges. The researchers evaluated several time series forecasting models, including group method of data handling (GMDH), long short-term memory (LSTM), adaptive neuro-fuzzy inference system (ANFIS), and various ensemble learning models. They found that integrating wavelet transforms with these models improved prediction accuracy, with the wavelet-ANFIS model achieving the best performance. In [29] the Christiano-Fitzgerald filter was combined with the GMDH to predict faults in contaminated insulators.

Studies of the contamination process that leads to the development of flashover, such as the one presented by Jin et al. [30] are rarer. Especially when it comes to applications of ML models, as presented by Zhang et al. [31], or hybrid methods for time series forecasting. In other applications, some authors have researched how to better identify faults based on time series analysis, as presented in Table 2.

Several authors (see Table 2) presented hybrid methods for predicting time series, such as CNN-LSTM, which uses CNN for feature extraction and LSTM for time series forecasting, showing that combining techniques with different objectives can improve the architecture, resulting in a hybrid approach that outperforms the lasted architectures for time series forecasting. A more detailed discussion of which state-of-the-art models are used for time series forecasting is presented in the next subsection.

### *2.1. State-of-the-Art in Time Series Forecasting*

In recent years, advances in ML and DL models have driven the development of more robust and accurate methods to predict time series. In this regard, DL-based approaches including recurrent neural networks (RNN) [54] and transformers [55], have shown promising performance. In [56] the authors considered the use of the temporal fusion transformer (TFT) model for time series. This model is an attention-based deep neural network architecture designed for multi-horizon time series forecasting, combining high performance with interpretability. The model incorporates static covariate encoders, gating mechanisms, variable selection networks, and hybrid temporal processing, which uses LSTMs for local patterns and self-attention to capture long-term dependencies.

Oreshkin et al. [57] proposed the neural basis expansion analysis for time series forecasting (N-BEATS), which is a deep neural network architecture designed for univariate time series forecasting based on residual connections and multiple fully connected layers. The deep temporal convolutional network (DeepTCN) was proposed in [58] and is a CNN architecture developed for probabilistic forecasting of multiple related time series. The model employs dilated causal convolutions, which guarantee dependence only on past inputs and capture long-range patterns

Table 2: Fault prediction and anomaly detection using ML approaches considering time series.

Work	Method	Application
[32]	Parallel time series modeling with LightNet and DarkNet.	Fault detection on intelligent vehicles.
[33]	Error fusion of multiple sparse auto-encoder LSTM.	Mechanical fault prediction.
[34]	Attention-based-LSTM, random forest, and extra-tree.	Machinery fault prediction.
[35]	CNN, gated recurrent unit (GRU), attention, and knowledge graph.	Machinery fault diagnosis.
[36]	Multiple time-series CNN.	Fault in semiconductor.
[37]	Masked spatial graph attention network with GRU.	Fault detection for unmanned aerial vehicles.
[38]	Time series transformer.	Machinery fault diagnosis.
[39]	Unsupervised deep autoencoder with dimension fusion function.	Fault detection in aero-engines.
[40]	Gaussian-linearized transformer with decomposition.	Fault diagnosis in methane gas sensors.
[41]	CNN-LSTM with attention.	Wind turbine fault prediction.
[42]	CNN-LSTM with one-class support vector machine (SVM).	Fault detection in multivariate complex process systems.
[43]	Standard LSTM and an LSTM autoencoder with a one-class SVM.	Anomaly detection in supply chain management.
[44]	Spatial and temporal attention-based GRU with seasonal-trend decomposition.	Fault diagnosis of electro-mechanical actuators.
[45]	Autoformer enhanced by Dilated loss module.	Potential bushing and transformer faults.
[46]	Multi-scale CNN and LSTM.	Bearing fault diagnosis.
[47]	Wavelet tranform with LSTM.	Fault in power grids.
[48]	Linear regression, support vector regression, multilayer Perceptron, deep neural network, and RNNs.	Failure prediction in contaminated insulators.
[49]	Ensemble random subspace with Hodrick–Prescott filter.	Fault forecasting in pin-type insulators.
[50]	EWT-sequence-to-sequence-LSTM with attention mechanism.	Insulators fault prediction.
[51]	Stacking ensemble learning model with wavelet transform.	Insulators contamination forecasting.
[52]	Bootstrap aggregation with Christiano–Fitzgerald random walk filter.	Fault prediction based on leakage current.
[53]	Adaptive neuro-fuzzy inference system with wavelet packets transform.	Insulator fault forecasting.

with computational efficiency. DeepTCN demonstrates robustness outperforming models such as seasonal autoregressive integrated moving average, light gradient boosting machine [59], and the probabilistic forecasting with autoregressive recurrent network [60].

In [61] the authors presented the multivariate time series forecasting with a graph neural networks model. This is a graph neural network designed-based model to forecast multivariate time series by learning the underlying graph structure. Its architecture combines three main components: a graph learning layer, which extracts dynamic relationships between series without the need for a predefined graph structure; graph convolution modules, which model spatial dependencies between variables; and temporal convolution modules, which capture long-term patterns through dilated convolutions, making it a robust approach for spatiotemporal forecasting in different datasets types.

Yu et al. [62] proposed the spatiotemporal graph convolutional network (STGCN), which is a DL architecture designed for traffic prediction, combining graph convolutions and temporal convolutions with gated linear units to efficiently model spatial and temporal dependencies. The architecture is composed of spatiotemporal convolutional blocks, where causal temporal convolutions extract sequential patterns and graph convolutions capture spatial relationships without relying on a fixed grid structure. STGCN is computationally efficient, enabling fast and scalable training for large networks. The model outperformed other approaches such as full-connected LSTM and graph convolutional GRU in several error metrics such as mean absolute error (MAE), mean absolute percentage error (MAPE), and root-mean-square error (RMSE), consuming up to 14 times less training time compared to state-of-the-art models.

In [63] the authors claim that using hybrid models can improve time series forecasting. The hybrid model proposed by the authors combines CNNs, attention-based LSTM (A-LSTM), and an auto-regressive model (AR) to forecast energy generation from multiple renewable sources. CNN captures spatial correlations between energy sources, A-LSTM models non-linear temporal patterns, and AR extracts linear trends. Its main advantages include the ability to model capture complex temporal patterns and predictive superiority over traditional models such as artificial neural networks and decision trees. The model also demonstrated a significant reduction in prediction errors compared to previous state-of-the-art approaches, reducing MAE by up to 27.1% and MAPE by 53.6% for photovoltaic solar energy. The high  $R^2$  values ( $>0.945$ ) confirm its good fit with the observed data, making it a robust and effective solution for forecasting renewable energy.

Mohammadi et al. [64] employed the EWT high-order fuzzy cognitive map that is also a hybrid model for forecasting time series that combines the EWT, high-order fuzzy cognitive maps (HFCM), and ridge regression. The model's architecture decomposes the time series data with EWT, which adapts filters to the signal spectrum, followed by modeling with HFCM, which captures long-term temporal dependencies, and hyperparameter optimization with ridge regression, avoiding overfitting. The forecast is reconstructed using inverse EWT, allowing complex patterns in non-stationary series to be captured. Evaluated with RMSE on 15 real data sets, the model outperformed 11 state-of-the-art algorithms, including LSTM, RNN, ANFIS, temporal convolutional network (TCN), and CNN-fuzzy cognitive maps.

Jin et al. [65] proposed a time series forecasting by reprogramming large language models (time-LLM) framework to predict time series, without modifying the backbone language model. The approach transforms time series into prototypical textual representations and uses the prompt-as-prefix technique to improve the input context. Its main advantages include generalization to multiple domains, data efficiency, advanced reasoning capabilities, and no need for fine-tuning, allowing robust predictions even with few examples or in zero-shot learning scenarios. Evaluated on different datasets, time-LLM outperformed conventional models in metrics such as mean-square error, MAE, symmetric MAPE (SMAPE), and overall weighted

average, demonstrating high accuracy in short and long-term forecasts.

In [66] proposes the use of CNN-LSTM for wind energy forecasting, with advanced hyperparameter optimization to improve accuracy and efficiency. CNN is used to extract spatial patterns from the data, while LSTM models short- and long-term temporal dependencies. Different hyperparameter optimization algorithms are evaluated, with Bayesian optimization via TPE being the most common approach. The results show that the advanced selection of hyperparameters significantly improves the effectiveness of wind energy forecasting, making the models more reliable.

These studies underscore the importance of integrating advanced analytical methods, such as ML and signal processing, with traditional monitoring techniques to improve fault prediction in distribution grid insulators. Continued research in this area is essential to develop more accurate and reliable predictive models, ultimately contributing to the improved stability and efficiency of power distribution grids.

### 3. Methodology

This paper considers the use of a filter input stage for noise attenuation and a hypertuned LLM model for time series forecasting. The time series is denoised to remove high frequencies and to have the focus of the analysis on the variation trend. To ensure that an optimal structure is assumed, the hyperparameters of the LLM are tuned via multi-criteria optimization based on TPE using the Optuna framework [67]. In this section, all considered techniques employed in the proposed optimized LLM model are explained.

#### 3.1. Input Stage Filter

Filters are applied in this paper to reduce the high frequencies in the signal, thus focusing on predicting the trend, which represents the most significant variation in the temporal analysis that leads to failure after a certain time in conditions of high contamination. The decomposition is expressed as:

$$y_t = \tau_t + s_t + \epsilon_t, \tag{1}$$

where  $\tau_t$  is the trend component,  $s_t$  is the seasonal (cyclical) component, and  $\epsilon_t$  is the remainder (residual) component [68]. The focus of the prediction here is the  $\tau_t$  because its variation represents the increase in the leakage current until it reaches the limit accepted by the insulator.

The CF, HP, STL, MSTL, EWT, Butterworth, and EDM filters are analyzed for signal denoising, and the best filter is employed in the model input stage. The symbols used in the equation of these filters are presented in Table 3. The symbols that are used in both the filters and the model are presented in the section that explains the model architecture.

##### 3.1.1. Christiano Fitzgerald Asymmetric Random Walk (CF) Filter

The CF filter is designed for the decomposition of time series data into seasonal and trend components. Unlike symmetric filters, the CF filter can operate asymmetrically, making it useful for real-time forecasting. The CF filter is based on the concept of band-pass filtering, where the goal is to isolate cycles within a specified frequency range [69]. The mathematical foundation of the filter involves approximating the ideal band-pass filter, which has a transfer function defined as:

$$H(\omega) = \begin{cases} 1 & \text{if } \kappa_{\text{lower}} \leq |\omega| \leq \kappa_{\text{upper}}, \\ 0 & \text{otherwise,} \end{cases} \tag{2}$$

Symbol	Definition
$a, b$	Coefficients of the filter
$c$	Intrinsic mode function
$e$	Envelop of the IMFs
$h$	Candidate IMF
$m$	Envelopes of envelopes
$n$	Order of the filter
$p$	Lower filter window
$q$	Upper filter window
$s$	Seasonal component
$w$	Filter weights
$F$	Fourier transform
$H$	Transfer function
$M$	Number of seasonal components
$N$	Number of modes of decomposition
$P$	Degree of the polynomial
$S$	Laplace transform variable
$T$	Sampling period
$W$	Empirical wavelet component
$Z$	Complex variable in the $z$ -domain
$\beta$	Coefficient of the polynomial
$\delta$	Width of the transition band
$\epsilon$	Residual component
$\kappa$	Cutoff frequency
$\lambda$	Smoothing hyperparameter
$\tau$	Trend component
$\phi$	Scaling function
$\psi$	Wavelet function
$\omega$	Angular frequency

Table 3: Symbols used in filter equations.

where  $\kappa_{\text{lower}}$  and  $\kappa_{\text{upper}}$  are the lower and upper cutoff frequencies, respectively. The filter is implemented as:

$$\hat{s}_t = \sum_{j=-p}^q w_j y_{t-j}, \quad (3)$$

where  $y_t$  is the observed time series,  $\hat{s}_t$  is the estimated seasonal component,  $w_j$  are the filter weights, and  $p$  and  $q$  define the range of the filter window. The weights  $w_j$  are determined by minimizing the error between the filtered signal and the ideal band-pass filter. Mathematically, this involves solving:

$$\min_{w_j} \int_{-\pi}^{\pi} \left| H(\omega) - \sum_{j=-p}^q w_j e^{-i\omega j} \right|^2 d\omega. \quad (4)$$

When future observations are not available, necessitating the use of an asymmetric filter, the CF filter solves this by adjusting the weights such that:

$$\hat{s}_t = \sum_{j=0}^q w_j y_{t-j}, \quad (5)$$



where only past and present observations are used. The computation of these asymmetric weights involves a recursive approach to approximate the frequency response of the ideal band-pass filter. The CF filter provides a robust method for decomposing and forecasting time series data in real-time applications [29].

### 3.1.2. Hodrick-Prescott (HP) Filter

The HP filter is used in time series analysis to decompose a series into its trend and seasonal components. It is particularly for extracting the smooth long-term trend from noisy data [70]. The HP filter decomposes a time series  $y_t$  into trend  $\tau_t$  and seasonal  $s_t$  components, previously defined in Eq. (1). The estimation of  $\tau_t$  is formulated as a minimization problem. Specifically, the objective function combines a goodness-of-fit term and a smoothness penalty:

$$\min_{\{\tau_t\}} \sum_{t=1}^T (y_t - \tau_t)^2 + \lambda \sum_{t=2}^{T-1} [(\tau_{t+1} - \tau_t) - (\tau_t - \tau_{t-1})]^2. \quad (6)$$

where the first term,  $\sum_{t=1}^T (y_t - \tau_t)^2$ , ensures that the estimated trend  $\tau_t$  fits the data well. The second term,  $\sum_{t=2}^{T-1} [(\tau_{t+1} - \tau_t) - (\tau_t - \tau_{t-1})]^2$ , penalizes changes in the slope of the trend, effectively ensuring that  $\tau_t$  is smooth over time. The smoothing hyperparameter  $\lambda$  controls the trade-off between these two objectives.

The choice of  $\lambda$  is subjective and may affect the decomposition. This issue can be solved with a  $\lambda$  adjustment. When  $\lambda \rightarrow 0$ , the trend  $\tau_t$  closely follows the original series  $y_t$ , allowing for greater flexibility, on the other hand, when  $\lambda \rightarrow \infty$ , the trend becomes a linear function, as the penalty on deviations from linearity dominates [71].

### 3.1.3. Season-Trend Decomposition using LOESS (STL) Filter

The operation in STL decomposition is based on the application of LOESS, a regression method used to estimate a smooth function by fitting weighted local polynomials [72]. The LOESS procedure at any time point  $t$  involves: Initially, it defines the neighborhood around  $t$  by selecting points within a specified window determined by the smoothing hyperparameter  $\lambda$ , which controls the fraction of data used in the local fit. Thus, the weights are assigned to the observations within the neighborhood based on their distances from  $t$  using a kernel function, commonly the tricube kernel:

$$w(x) = (1 - |x|^3)^3, \quad \text{for } |x| \leq 1, \quad w(x) = 0, \text{ otherwise.} \quad (7)$$

Fitting a weighted polynomial (typically linear or quadratic) to the data within the neighborhood, minimizing the locally weighted sum of squared residuals, given by

$$\min_{\beta_0, \beta_1, \dots, \beta_P} \sum_i w(x_i) \left( y_i - \sum_{j=0}^P \beta_j x_i^j \right)^2, \quad (8)$$

where  $\beta_0, \beta_1, \dots, \beta_P$  are the coefficients of the polynomial, and  $P$  is the degree of the polynomial (commonly  $P = 1$  or  $P = 2$ ). Once the decomposition is complete, the trend component  $\tau_t$  can be used for forecasting. For example, future values of  $y_t$  may be predicted by evaluating the trend  $\tau_t$  using prediction models. The remainders are often modeled as a stochastic noise, assumed as white noise [73].

### 3.1.4. Multiple Season-Trend Decomposition using LOESS (MSTL) Filter

The MSTL is a method used for analyzing time series data, particularly when multiple seasonal components and trends are present. The primary goal of MSTL is to decompose the time series into trend, seasonality, and remainder components according to Equation 1. Mathematically, for a univariate time series  $y_t$ , the method can be represented as follows:

$$y_t = \tau_t + \sum_{j=1}^M s_{j,t} + \epsilon_t, \quad (9)$$

where  $s_{j,t}$  is the seasonal component for the  $j$ -th seasonal frequency, where  $j = 1, \dots, M$ , and  $M$  is the number of seasonal components [74].

Like the STL, the MSTL employs the concept of LOESS to estimate each component iteratively. LOESS operates by fitting a polynomial regression model locally for a subset of data points around each time index  $t$ , weighted by a kernel function [75]. The kernel assigns higher weights to points closer to  $t$  and lower weights to points farther away.

In the MSTL decomposition process, the seasonal components  $s_{j,t}$  are estimated first. Each seasonal component corresponds to a specific periodicity, and LOESS smoothing is applied after aggregating data for that periodicity. MSTL is robust to outliers through the use of LOESS, where weights are iteratively adjusted based on residuals to reduce the influence of extreme values [76].

### 3.1.5. Empirical Wavelet Transform (EWT) Filter

The EWT is a signal decomposition method that is designed to extract meaningful frequency components from a signal. Unlike traditional wavelet transforms, which rely on predefined mother wavelets and fixed frequency partitions, the EWT constructs wavelet filters based on the spectral characteristics of the input signal. This adaptability makes it a promising method for time series forecasting, especially in cases where signals exhibit non-stationary behavior [77].

For each segment  $[\omega_{k-1}, \omega_k]$ , a scaling function  $\phi_k(\omega)$  and a wavelet function  $\psi_k(\omega)$  are constructed. These functions are designed to satisfy orthogonality and completeness conditions over the defined frequency intervals. The  $\phi_k(\omega)$  is used to capture the low-frequency components, while the  $\psi_k(\omega)$  isolates the band-limited frequency components [78]. The empirical scaling function and wavelet function in the Fourier domain can be defined as:

$$\phi_k(\omega) = \begin{cases} 1, & \omega \in [0, \omega_k - \delta_k], \\ \cos\left(\frac{\pi}{2\delta_k}(\omega - (\omega_k - \delta_k))\right), & \omega \in [\omega_k - \delta_k, \omega_k], \\ 0, & \text{otherwise,} \end{cases} \quad (10)$$

$$\psi_k(\omega) = \begin{cases} 1, & \omega \in [\omega_{k-1} + \delta_k, \omega_k - \delta_k], \\ \sin\left(\frac{\pi}{2\delta_k}(\omega - (\omega_{k-1} + \delta_k))\right), & \omega \in [\omega_{k-1}, \omega_{k-1} + \delta_k], \\ \cos\left(\frac{\pi}{2\delta_k}(\omega - (\omega_k - \delta_k))\right), & \omega \in [\omega_k - \delta_k, \omega_k], \\ 0, & \text{otherwise,} \end{cases} \quad (11)$$

where  $\delta_k$  is the width of the transition band.

After constructing the wavelet and scaling functions, the signal  $x(t)$  is decomposed into empirical wavelet coefficients using the inverse Fourier transform. The  $k$ th empirical wavelet component is given by:

$$W_k(t) = F^{-1} [\hat{x}(\omega)\psi_k(\omega)], \quad (12)$$

where  $F^{-1}$  denotes the inverse Fourier transform. Similarly, the residual low-frequency component is captured by:

$$s_N(t) = F^{-1} [\hat{x}(\omega)\phi_N(\omega)]. \quad (13)$$

Thus, the original signal can be reconstructed as the sum of the decomposed components:

$$x(t) = s_N(t) + \sum_{k=1}^N W_k(t). \quad (14)$$

The EWT is particularly advantageous for time series forecasting as it effectively isolates the dominant modes of variability, allowing for independent modeling of each component. This modularity facilitates the application of predictive models, such as prediction models, neural networks, or hybrid approaches, on each extracted component [79].

### 3.1.6. Butterworth Filter

The Butterworth filter is a signal processing technique used in time series analysis and forecasting due to its smooth frequency response and minimal distortion characteristics. It effectively separates high-frequency noise from low-frequency trends in time series data. The Butterworth filter is applied to have a maximally flat magnitude response in the passband, avoiding ripples in the frequency response [13]. The general transfer function for an  $n$ th-order Butterworth filter is given by:

$$H(\omega) = \frac{1}{\sqrt{1 + \left(\frac{\omega}{\kappa}\right)^{2n}}}, \quad (15)$$

where  $\omega$  is the angular frequency,  $\kappa$  is the cutoff frequency, and  $n$  is the order of the filter. The cutoff frequency  $\kappa$  defines the boundary between the passband and the stopband. The filter's order,  $n$ , defines the steepness of the transition between the passband and the stopband. Higher-order filters yield sharper transitions but introduce higher computational complexity [80].

In time series forecasting, the Butterworth filter is often used as a low-pass filter to extract the low-frequency trend component of a time series. This is accomplished by suppressing high-frequency variations, which are typically associated with noise or short-term fluctuations while retaining the underlying trend [81]. To apply the Butterworth filter to discrete time series data, the transfer function is transformed into the  $Z$ -domain using the bilinear transformation:

$$S = \left(\frac{2}{T}\right) \frac{1 - Z^{-1}}{1 + Z^{-1}}, \quad (16)$$

where  $S$  is the Laplace transform variable,  $T$  is the sampling period, and  $Z$  is the complex variable in the  $Z$ -domain. Substituting this transformation into the continuous-time transfer function yields the discrete-time transfer function:

$$H(Z) = \frac{\sum_{k=0}^n b_k Z^{-k}}{1 + \sum_{k=1}^n a_k Z^{-k}}, \quad (17)$$

where the coefficients  $a_k$  and  $b_k$  are determined by the order of the filter and the cutoff frequency. The recursive form of this difference equation enables efficient implementation of the filter in time series forecasting applications [82].

The Butterworth filter minimizes distortion in the trend component by ensuring that the magnitude response in the passband is as flat as possible. This flexibility in adjusting the cutoff frequency and filter order allows it to be tailored to the specific characteristics of the time series under study, making it a powerful method for preprocessing and smoothing data before modeling and prediction [83].

### 3.1.7. Empirical Mode Decomposition (EMD) Filter

The EMD is an adaptive, data-driven technique for analyzing non-linear and non-stationary time series data. It decomposes a signal into a finite set of components called intrinsic mode functions (IMFs) and a residual. The decomposition process begins by identifying the IMFs, which are defined by two conditions: the number of extrema and zero crossings in an IMF must either be equal or differ at most by one, and the mean value of the upper envelope and the lower envelope must be zero at every point [84].

To formalize the process, consider a time series  $x(t)$ . The first step involves constructing envelopes for the signal using cubic splines to interpolate the local maxima and minima. Denoting the upper and lower envelopes as  $e_{\text{upper}}(t)$  and  $e_{\text{lower}}(t)$ , respectively, their mean  $m(t)$  is calculated as

$$m(t) = \frac{e_{\text{upper}}(t) + e_{\text{lower}}(t)}{2}. \quad (18)$$

The mean is then subtracted from the original signal to produce a candidate IMF:

$$h(t) = x(t) - m(t). \quad (19)$$

This process, known as sifting, is iterated until  $h(t)$  satisfies the IMF criteria. The first IMF ( $c_1(t)$ ), captures the highest frequency oscillations in the signal. To extract subsequent IMFs,  $c_1(t)$  is subtracted from the original signal:

$$\epsilon_1(t) = x(t) - c_1(t), \quad (20)$$

where  $\epsilon_1(t)$  becomes the new input signal for further decomposition. Repeating this procedure yields a set of IMFs  $\{c_1(t), c_2(t), \dots, c_n(t)\}$  and a final residual  $\epsilon_n(t)$ , such that

$$x(t) = \sum_{i=1}^n c_i(t) + \epsilon_n(t). \quad (21)$$

Each IMF isolates oscillatory modes of different scales, making EMD particularly suitable for analyzing signals where distinct temporal scales are present. For time series forecasting, consider that the extracted IMFs often exhibit simpler patterns than the original signal. These components can then be modeled independently using ML methods. Forecasting can proceed by predicting each IMF  $c_i(t)$  individually by ML models [85].

### 3.2. Prediction Model Architecture

LLM applied for time series, or timeLLM, is built upon the foundational structure of large language models by incorporating temporal reasoning directly into its architecture. The innovation of this model lies in the integration of temporal embeddings, dynamic contextual adjustments, and attention mechanisms for time-dependent data. These features enhance the model’s ability to handle sequential and time-sensitive information [86]. The symbols used in the equation of the model architecture and its hypertuning are presented in Table 4.

Symbol	Definition
$d$	Embedding dimension
$i, k$	Iteration
$l, g$	Conditional densities
$p$	Probability
$t$	Timestamps or step
$x$	Input data
$y$	Observed time series (objective)
$\gamma$	Quantile of the observed objective
$\eta$	Event in a sequence
$\mathcal{G}$	Gating function
$\mathcal{K}$	Kernel function
$\mathcal{L}$	Loss function
$\mathcal{N}$	Normalization constant
$\mathcal{X}$	Hyperparameter space
$\mathbf{h}$	Modified input representation
$\mathbf{v}$	Vector representation
$\mathbf{E}$	Standard token embedding
$\mathbf{K}$	Key matrix
$\mathbf{Q}$	Query matrix
$\mathbf{T}$	Temporal embedding
$\mathbf{V}$	Value matrix
$\mathbf{W}$	Time-aware weighting matrix

Table 4: Symbols used in model equations.

Temporal embeddings encode time-related information, such as timestamps or relative durations, by mapping these into a latent space. Mathematically, given a sequence of events  $\{\eta_1, \eta_2, \dots, \eta_m\}$  occurring at corresponding timestamps  $\{t_1, t_2, \dots, t_n\}$ , temporal embeddings  $\mathbf{T}(t)$  map each timestamp  $t_i$  to a vector representation  $\mathbf{v}_i \in \mathbb{R}^d$ , where  $d$  is the embedding dimension. These embeddings are learned jointly with the model hyperparameters, ensuring that temporal context is captured alongside linguistic features [87].

The temporal embeddings are integrated into the model’s transformer layers. For each input token  $x_i$ , the modified input representation is given by

$$\mathbf{h}_i = \mathbf{E}(x_i) + \mathbf{T}(t_i), \quad (22)$$

where  $\mathbf{E}(x_i)$  is the standard token embedding and  $\mathbf{T}(t_i)$  is the temporal embedding. This addition ensures that the model incorporates temporal information at the input stage.

The attention mechanism in timeLLM is adapted to prioritize temporal dependencies. The scaled dot-product attention is modified to include a temporal weighting term. For query  $\mathbf{Q}$ , key  $\mathbf{K}$ , and value  $\mathbf{V}$  matrices, the attention weights are computed as

$$\text{Attention}(\mathbf{Q}, \mathbf{K}, \mathbf{V}) = \text{softmax} \left( \frac{\mathbf{Q}\mathbf{K}^T}{\sqrt{d_k}} + \mathbf{W}_T \right) \mathbf{V}, \quad (23)$$

where  $\mathbf{W}_T$  is a time-aware weighting matrix that adjusts the attention based on temporal proximity [88]. Incorporating dynamic contextual awareness, timeLLM leverages time-dependent positional encodings and gating mechanisms. The model introduces a gating function  $\mathcal{G}(t)$  that modulates the influence of temporal embeddings based on the recency or relevance of information. The gated representation is computed as

$$\mathbf{h}'_i = \mathcal{G}(t_i) \cdot \mathbf{h}_i, \quad (24)$$

where  $\mathcal{G}(t_i)$  is a learnable function of  $t_i$ .

TimeLLM has practical applications in event forecasting, where it analyzes historical data to predict future outcomes. For example, given a time series  $\{(t_i, x_i)\}$  representing observed data points, the model learns to predict  $x_{n+1}$  by optimizing the loss function

$$\mathcal{L} = \sum_{i=1}^n (x_i - \hat{x}_i)^2 + \lambda \|\mathbf{T}(t)\|^2, \quad (25)$$

where the second term regularizes the temporal embeddings to prevent overfitting. By analyzing cross-attention patterns between temporally ordered inputs, timeLLM identifies dependencies that inform predictions and interpretations [89]. The incorporation of these mechanisms makes timeLLM a robust solution for time-sensitive applications, such as time series forecasting presented in this paper.

### 3.3. Model Hypertuning

For hyperparameter model tuning, the TPE is applied. TPE is a model-based optimization algorithm that builds on the Bayesian optimization, tailored for hyperparameter tuning [90]. The TPE algorithm uses probabilistic modeling to construct surrogate models of the objective function and guides the search for optimal hyperparameter configurations. In this paper, the TPE is applied for hypertuning the proposed optimized LLM model, the considered hyperparameters are the batch size, dropout, learning rate, and number of heads.

The goal of hyperparameter optimization is to minimize or maximize an objective function  $f : \mathcal{X} \rightarrow \mathbb{R}$ , where  $\mathcal{X}$  is the hyperparameter space [91]. The TPE idea relies on modeling the conditional probability  $p(y | x)$ , where  $x \in \mathcal{X}$  is a vector of hyperparameters and  $y = f(x)$  is the corresponding objective value. The TPE replace  $p(y | x)$  with two conditional densities,  $l(x)$  and  $g(x)$ , based on a threshold  $\gamma$  such that:

$$l(x) = p(x | y < \gamma), \quad g(x) = p(x | y \geq \gamma), \quad (26)$$

where  $\gamma$  is a quantile of the observed objective values  $\{y_1, y_2, \dots, y_n\}$ , often chosen as a fixed percentile. The TPE algorithm thus rewrites the marginal likelihood  $p(x | y)$  using Bayes' theorem:

$$p(x | y) = \begin{cases} l(x)p(y < \gamma)/\mathcal{N} & \text{if } y < \gamma, \\ g(x)p(y \geq \gamma)/\mathcal{N} & \text{if } y \geq \gamma, \end{cases} \quad (27)$$

where  $\mathcal{N} = p(y)$  is the normalization constant.

TPE focuses on maximizing the expected improvement (EI) by choosing hyperparameter configurations that are likely to improve upon the current best observations. The EI criterion is reformulated in TPE by using the ratio of densities  $l(x)/g(x)$ . Intuitively, TPE selects  $x$  to maximize this ratio, favoring regions of the search space that are more probable under  $l(x)$  (regions associated with good performance) while being less probable under  $g(x)$  (regions associated with worse performance) [92].

The algorithm constructs  $l(x)$  and  $g(x)$  using kernel density estimation (KDE). For a set of observed hyperparameter configurations  $\{x_1, x_2, \dots, x_n\}$  and their corresponding objective values  $\{y_1, y_2, \dots, y_n\}$ , the densities are modeled as:

$$l(x) = \sum_{i \in \mathcal{I}_l} w_i \mathcal{K}(x, x_i), \quad g(x) = \sum_{i \in \mathcal{I}_g} w_i \mathcal{K}(x, x_i), \quad (28)$$

where  $\mathcal{I}_l = \{i \mid y_i < \gamma\}$ ,  $\mathcal{I}_g = \{i \mid y_i \geq \gamma\}$ ,  $w_i$  are the weights associated with each sample, and  $\mathcal{K}(x, x_i)$  is a kernel function. The threshold  $\gamma$  is updated dynamically as new observations are added to the dataset.

By modeling  $l(x)$  and  $g(x)$  using KDE, TPE can efficiently handle complex, multimodal distributions over the hyperparameter space. Moreover, it exploits the tree-structured dependencies within  $x$  by breaking the optimization problem into sub-problems, each model with a separate density estimator. The hyperparameter configuration for the next evaluation is sampled by optimizing the acquisition function, which in TPE is the maximization of the density ratio:

$$x^* = \arg \max_{x \in \mathcal{X}} \frac{l(x)}{g(x)}. \quad (29)$$

This process is repeated iteratively, with each new observation refining the density estimators  $l(x)$  and  $g(x)$ , guiding the search toward better regions of the hyperparameter space. TPE is particularly effective for problems with hierarchical or conditional hyperparameter structures, making it well-suited for modern ML models [93].

In this paper, the Optuna framework is considered for the application of the TPE algorithm. The Monte Carlo approach is considered for analyzing different forecast horizons, this method relies on generating random numbers to explore a wide range of possible scenarios within a model, ensuring adequate random sampling [94]. The complete pipeline of the proposed optimized LLM method is presented in Figure 1.

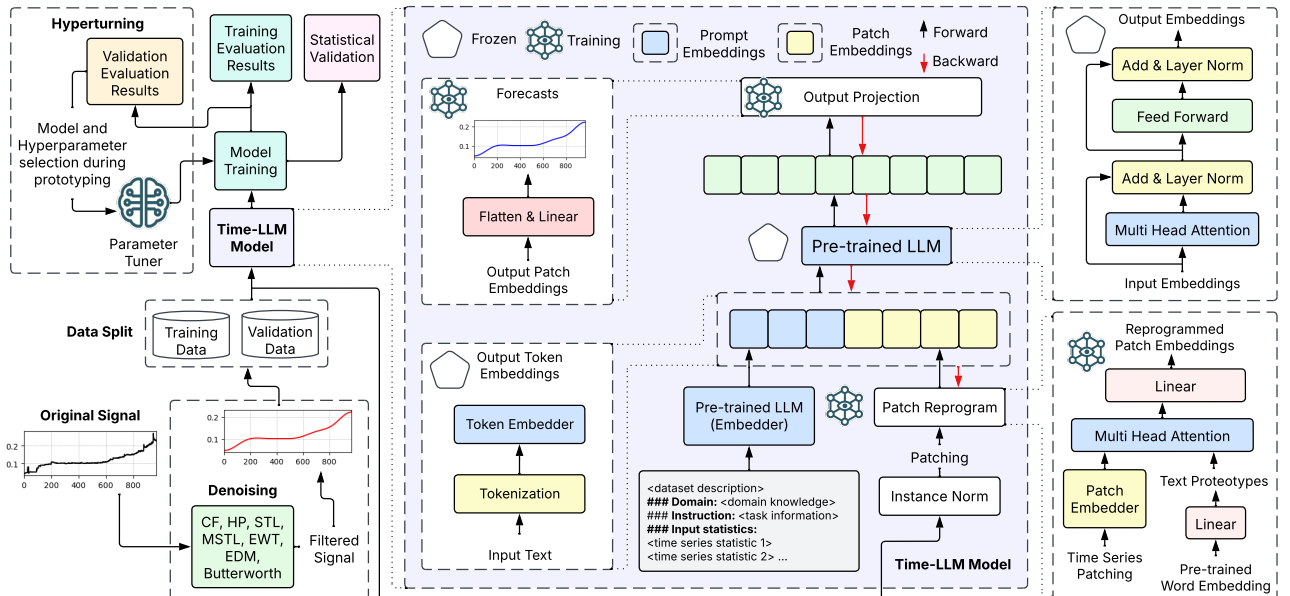


Figure 1: Proposed optimized LLM model.

## 4. Results and Discussion

This section presents the dataset used for the experiments, the analysis setup, the results of applying the proposed optimized LLM, and a benchmarking with other well-established DL methods. After defining the dataset and comparison settings used in this paper, the results of applying filters to reduce noise are discussed. From the filtered signal, the model is optimized using hypertuning. Once optimized, an analysis is handled concerning the variation in the forecast horizon, after which comparative results of the proposed model to other models are presented.

### 4.1. Dataset

The data set considered in this paper refers to leakage current measurements in an experiment on insulators subjected to artificial contamination. The experiment consists of increasing the level of contamination in insulators until a disruptive discharge occurs. The increase in contamination results in an increase in leakage current, which is the main indicator that a fault may occur [95]. Six insulators were evaluated in the experiment, four of which were discharged before the end of the experiment and were disregarded. Of the two insulators that withstood the increase in contamination without being discharged, only one had a linear increase in leakage current, and this was the insulator considered in this study.

To reduce the complexity of the analysis, a downsample is handled in the pre-preprocessing stage, which means that instead of 96,800 recorded records being considered, corresponding to 26.9 hours of evaluation, 968 are the focus of the analysis. Electrical discharges occurred in many insulators after the leakage current exceeded 200mA, which is an appropriate threshold for predicting that a fault will occur. The considered signal of the leakage current in the insulator in question is shown in Figure 2.

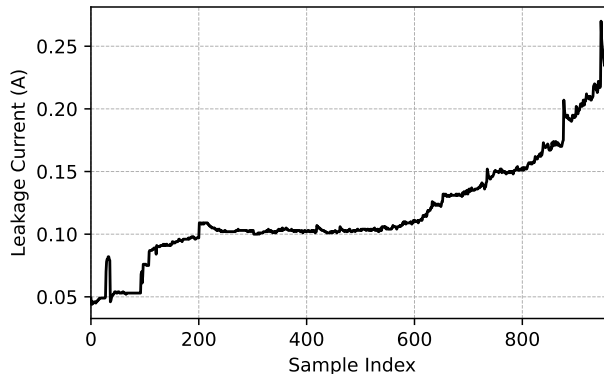


Figure 2: Leakage current in an insulator with artificial contamination.

The artificial contamination considered was applied in a high-voltage laboratory, in which a voltage of 8.66 kV RMS 60Hz was applied. The increase in contamination was handled following the IEC 60507 [95] standard, which is specific to this evaluation. LabVIEW software was used to monitor and save the leakage current values from the experiment. The insulators were fixed according to the power utility’s standards and were grounded to measure the current flowing through the ground.

### 4.2. Experiment Setup

The experiments utilized an NVIDIA RTX 3060 TI graphics processing unit with 120 GB of random-access memory. The models were implemented in Python. Processing time encompasses the total duration required for both model training and testing. The evaluation metrics include RMSE, MAE, MAPE, and SMAPE, defined as follows:



$$\text{RMSE} = \sqrt{\frac{1}{n} \sum_{i=1}^n (y_i - \hat{y}_i)^2}, \quad (30)$$

$$\text{MAE} = \frac{1}{n} \sum_{i=1}^n |y_i - \hat{y}_i|, \quad (31)$$

$$\text{MAPE} = \frac{100\%}{n} \sum_{t=1}^n \left| \frac{y_i - \hat{y}_i}{y_i} \right|, \quad (32)$$

$$\text{SMAPE} = \frac{100\%}{n} \sum_{i=1}^n \frac{|y_i - \hat{y}_i|}{(|y_i + \hat{y}_i|)/2}, \quad (33)$$

where  $y_i$  is the actual value,  $\hat{y}$  is the forecasted value, and  $n$  is the number of observations.

To have a comparative assessment of the proposed optimized LLM, the standard RNN, dilated RNN, LSTM, GRU, TFT, TCN, informer, DeepNPTS, N-BEATS, and NHITS models are evaluated. In the analysis of different forecast horizons, considering multiple LLM models, the Monte Carlo approach was applied with a step equal to 5, from the initial horizon to the last horizon evaluated.

The comparative analysis considered multi-horizon prediction, taking into account a horizon of 5 to 60 steps ahead (short-term and medium-term horizons). Each sample in the experiment considers the signal recorded at a time step of one second. The experiment, which lasted a few hours, represents the accumulation of contaminants that would occur in an external environment over approximately thirty years. The time it takes for a fault to develop depends heavily on the characteristics of the location where the system is installed.

### 4.3. Filtering Analysis

In the pre-processing stage, to ensure a fair analysis, all the filters considered in this paper are applied using their default settings. The results of this evaluation in relation to the original signal are shown in Figure 3. This figure shows the sample index as the horizontal axis, since the downsample is applied to reduce the complexity of the analysis.

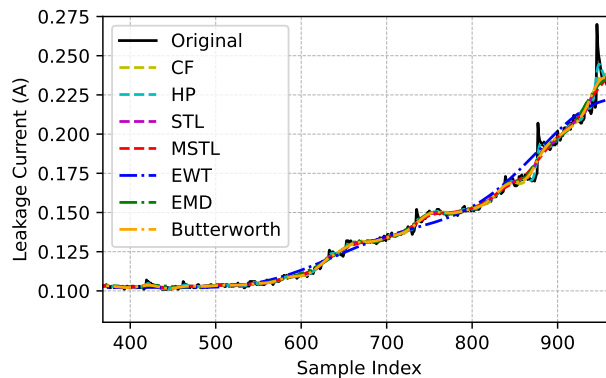


Figure 3: Comparison of application of filters to the original signal.

Based on these results, the timeLLM model is applied to the original signal and the denoised signals by all the filters, as shown in Table 5. In this analysis, the default setup is used in the model considering a horizon equal to 60 steps ahead. The time needed to process the model with each of the filters was equivalent since the greatest computational effort is regarding the training stage of the DL model, not the usage of the filter.

Table 5: Results of timeLLM using different filters.

Filter	RMSE	MAE	MAPE	SMAPE	Time (s)
Original	$6.06 \times 10^{-3}$	$4.63 \times 10^{-3}$	$3.33 \times 10^{-2}$	3.42	$1.24 \times 10^1$
CF	$5.52 \times 10^{-3}$	$4.32 \times 10^{-3}$	$3.12 \times 10^{-2}$	3.20	$1.27 \times 10^1$
HP	$5.38 \times 10^{-3}$	$4.23 \times 10^{-3}$	$3.05 \times 10^{-2}$	3.13	$1.28 \times 10^1$
STL	$5.15 \times 10^{-3}$	$3.95 \times 10^{-3}$	$2.85 \times 10^{-2}$	2.92	<b><math>1.23 \times 10^1</math></b>
MSTL	$5.63 \times 10^{-3}$	$4.56 \times 10^{-3}$	$3.29 \times 10^{-2}$	3.38	$1.25 \times 10^1$
EWT	<b><math>3.15 \times 10^{-3}</math></b>	<b><math>2.99 \times 10^{-3}</math></b>	<b><math>2.25 \times 10^{-2}</math></b>	<b>2.28</b>	$1.25 \times 10^1$
EMD	$5.27 \times 10^{-3}$	$3.69 \times 10^{-3}$	$2.64 \times 10^{-2}$	2.71	<b><math>1.23 \times 10^1</math></b>
Butterworth	$5.04 \times 10^{-3}$	$3.86 \times 10^{-3}$	$2.79 \times 10^{-2}$	2.86	$1.28 \times 10^1$

Best results in bold

Considering the pre-defined setup of the filtering techniques, the best results were found using EWT, as the RMSE is equal to  $3.15 \times 10^{-3}$ , MAE equal to  $2.99 \times 10^{-3}$ , MAPE equal to 2.25%, and a SMAPE equal to 2.28. It is important to note that all these filters could be applied at this stage, but fine-tuning is required for each specific filter.

The results of using all the filters were superior to the results obtained by the base model without using the filter, showing that their application is promising where the model using the EWT filter showed, in general, lower errors than the other filters and the original data. In the following subsection, the model hypertuning evaluation is presented.

#### 4.4. Hypertuning Analysis

An important definition to be made in the model’s tuning phase is the variability space (gap) of each hyperparameter. If the space is not properly defined, the model may struggle to find the optimum. A large search space makes it difficult to optimize the hyperparameters, and a small space can limit the search, causing the TPE to find values near the extreme of variation for each hyperparameter.

To ensure that the model has been properly optimized, hypertuning with a large search space has been done beforehand, so the search space presented here takes into account the gap of best values found in the first experiment. Considering the gap of the first experiment, the hypertuning is done with the following values of batch size [10 to 20], number of heads [1 to 8], learning rate [0.001 to 0.01], and dropout [0.0 to 0.7]. The results of this analysis are shown in Figure 4. This analysis considered a time-LLM model with the EWT filter, using a horizon and input size equal to 20. Considering that all the optimal results of the hyperparameters evaluated were within the variation gap analyzed, the analysis was carried out properly.

In Figure 4, the black dots represent the local minima of the gradient of each combination, considering Eq. (30) as the loss function. The lighter the gradient (white being the lightest color), the greater the loss function result and, in turn, the worse the result obtained. Conversely, the darker the color of the gradient (in this case dark blue), the lower the loss function result and, in turn, the better the result, since in both cases the optimization function is to reduce the RMSE.

In this optimization, the batch size hyperparameter had an importance of 13% in achieving the goal of reducing the RMSE, the learning rate had an importance of 17%, the number of heads in the model had an importance of 19%, and the dropout had an importance of 51%, making it the most important hyperparameter to optimize.

The rank of the hyperparameter fitting attempts is shown in Figure 5. The values in the center of the plots are linear, as they only show the variation of one hyperparameter at a time. It should be noted that, for this case, the redder it gets, the higher the loss function (RMSE in this case), and, in turn, the worse the approximation of the output to the ground truth.

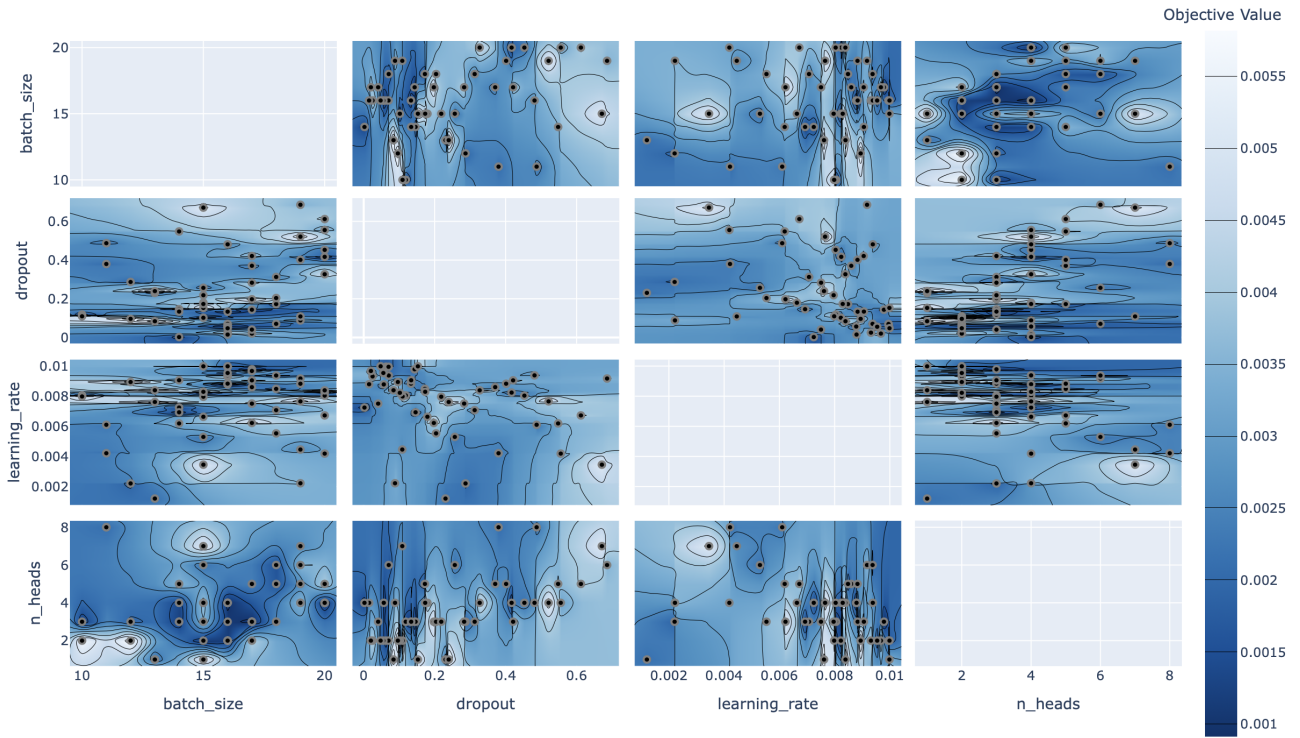


Figure 4: Results of multi-objective optimization.

Similarly, the lower the value of the loss function, the color will tend toward dark blue, and the closer the output model will be to the ground truth.

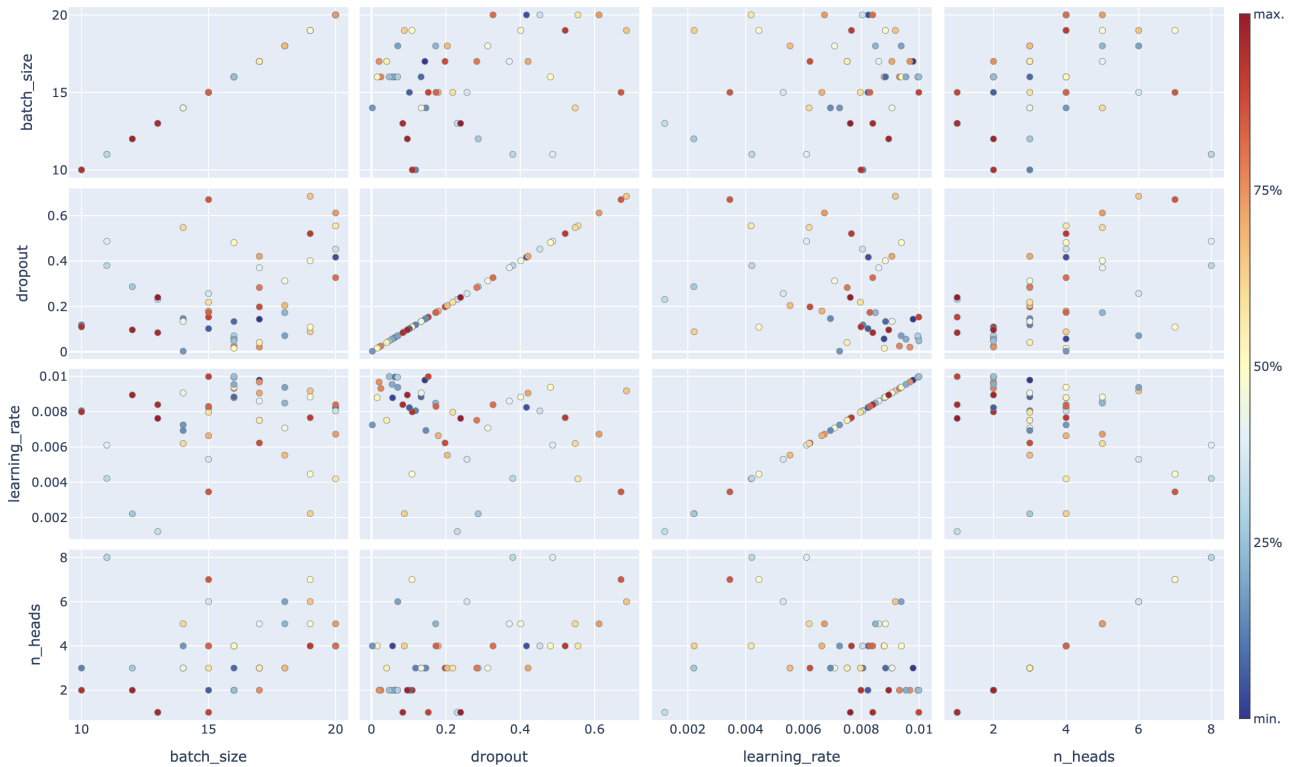


Figure 5: Trial rank of hyperparameters.

Multi-criteria optimization tries interactively to find the best hyperparameter setting to minimize the objective function, reducing the RMSE in this paper, by finding an optimum that

combines the setting of several hyperparameters simultaneously. The optimum values found in this experiment were a batch size of 17, using 3 heads, a learning rate of  $9.77 \times 10^{-3}$ , and a dropout equal to  $1.43 \times 10^{-1}$ , this hyperparameter setup was used for the following analyses, this being the optimized model.

Figure 6 presents the different combinations between different variables and the lighter the color of the combination, the higher the loss function value and, consequently, the worse the model result. The darker the color of the combination between different variables (dark blue in this case), the lower the loss function value and therefore the better the model output.

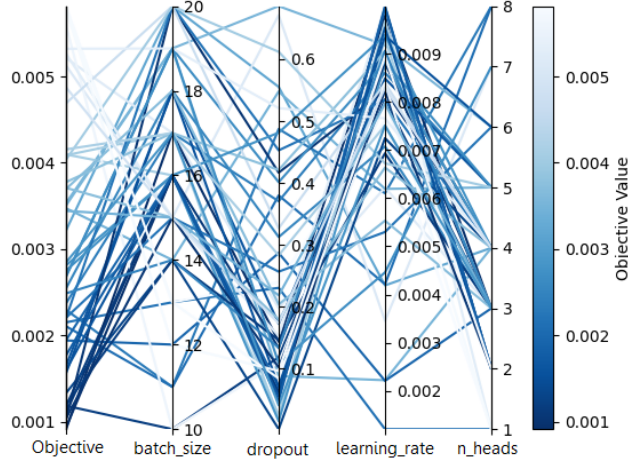


Figure 6: Model trails in hypertuning.

An interesting observation in this presentation (Figure 6) is that many values are close in the trials. This shows an advantage in the application of TPE since when the value of the hyperparameter is getting close to the optimum, the algorithm creates new, more assertive trials for multi-criteria optimization. Other hypertuning techniques, such as random sampling, can have a larger search space, but because they are random trials, fewer values close to the optimum are evaluated.

#### 4.5. Multi-horizon Analysis

The purpose of the evaluation of horizons is to analyze the impact using a longer forecast horizon has on the model’s performance. To this end, Table 6 presents a comparative analysis of various forecast horizons using the proposed optimized LLM model using the EWT as the input stage filter. A forecast of 5 steps ahead is considered a short-term horizon, and 60 steps ahead is considered a medium-term horizon.

The results of this comparison showed that the longer the forecast horizon, the more difficult it is to produce a forecast with lower error. The time needed to train the model and carry out the test did not vary considerably when changing the forecast horizon, but the error had a big impact, showing how challenging it is to carry out forecasts with long forecast horizons.

The MAPE values show that the model struggles to make predictions for horizons greater than 20 steps ahead since the values were higher than 30%. This challenge is related to the variability of the data, where non-linear time series are more difficult to predict in horizons that consider many steps ahead. This result shows that the proposed model is better suited to short-term than medium-term horizons.

A visualization of the variation in the model’s performance as the forecast horizon increases can be seen in Figure 7. For random sampling, a Monte Carlo approach is considered to train the model. The model shows a considerably promising result up to a Horizon equal to 20 steps ahead, after which greater difficulties are encountered in handling the forecast, especially after

Table 6: Time step horizon analysis.

Horizon	RMSE	MAE	MAPE	SMAPE	Time (s)
05	<b><math>2.24 \times 10^{-4}</math></b>	<b><math>1.84 \times 10^{-4}</math></b>	<b><math>1.41 \times 10^{-3}</math></b>	<b><math>1.41 \times 10^{-1}</math></b>	<b><math>1.67 \times 10^1</math></b>
10	$3.58 \times 10^{-4}$	$2.95 \times 10^{-4}$	$2.25 \times 10^{-3}$	$2.25 \times 10^{-1}$	$1.68 \times 10^1$
15	$4.50 \times 10^{-4}$	$3.84 \times 10^{-4}$	$2.90 \times 10^{-3}$	$2.91 \times 10^{-1}$	<b><math>1.67 \times 10^1</math></b>
20	$4.62 \times 10^{-4}$	$3.77 \times 10^{-4}$	$2.84 \times 10^{-3}$	$2.85 \times 10^{-1}$	$1.68 \times 10^1$
25	$5.79 \times 10^{-4}$	$4.98 \times 10^{-4}$	$3.76 \times 10^{-3}$	$3.77 \times 10^{-1}$	$1.71 \times 10^1$
30	$2.82 \times 10^{-3}$	$2.61 \times 10^{-3}$	$1.95 \times 10^{-2}$	$1.97 \times 10^{-1}$	<b><math>1.67 \times 10^1</math></b>
35	$5.87 \times 10^{-4}$	$4.40 \times 10^{-4}$	$3.27 \times 10^{-3}$	$3.26 \times 10^{-1}$	$1.70 \times 10^1$
40	$1.32 \times 10^{-3}$	$1.07 \times 10^{-3}$	$7.86 \times 10^{-3}$	$7.82 \times 10^{-1}$	$1.68 \times 10^1$
45	$1.41 \times 10^{-3}$	$1.21 \times 10^{-3}$	$8.90 \times 10^{-3}$	$8.85 \times 10^{-1}$	<b><math>1.67 \times 10^1</math></b>
50	$1.02 \times 10^{-3}$	$8.54 \times 10^{-4}$	$6.27 \times 10^{-3}$	$6.25 \times 10^{-1}$	$1.68 \times 10^1$
55	$1.54 \times 10^{-3}$	$1.19 \times 10^{-3}$	$8.66 \times 10^{-3}$	$8.60 \times 10^{-1}$	$1.70 \times 10^1$
60	$1.21 \times 10^{-3}$	$9.30 \times 10^{-4}$	$6.77 \times 10^{-3}$	$6.73 \times 10^{-1}$	$1.68 \times 10^1$

Best results in bold

35 steps ahead, this result is expected because the longer the horizon, the more difficult it becomes to predict the variation.

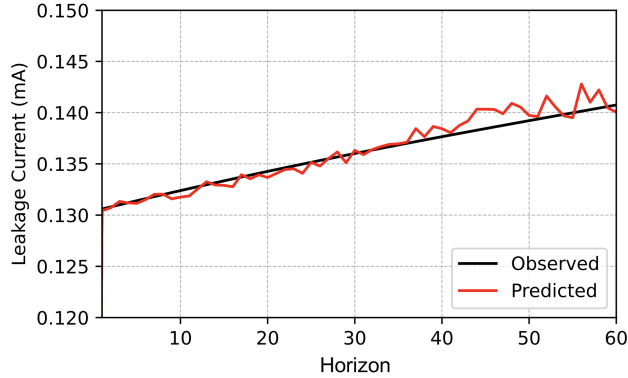


Figure 7: Forecast results versus the original signal for different prediction horizons.

#### 4.6. Statistical Analysis

To perform a statistical analysis, the proposed optimized LLM model was computed for 50 runs with different initialization weights (seed). The result of this evaluation is shown in Table 7. The mean, median, mode, range, standard deviation, 25th, 50th, and 75th percentile (%ile), interquartile range (IQR), skewness, and kurtosis for each performance metric (RMSE, MAE, MAPE and SMAPE) are presented. In general, the results of the statistical analysis show that the model has promising average values, making it a suitable model for the task discussed here.

To give a visual presentation of the variability of the results in relation to the 50 runs, Figure 8 shows a box plot of the errors evaluated in this paper using the proposed optimized LLM model. This presentation shows some outliers with greater error than the average values obtained by the model.

Considering that the initialization of the weights is random and that the vast majority of the results are close to the average (observing a logarithmic presentation), the results are promising. These results show that the model is stable, and based on that, a final comparative analysis is presented in the following.

Table 7: Statistical performance of the hypertuned EWT-LLM considering 50 runs.

Metrics	RMSE	MAE	MAPE	SMAPE
Mean	$1.61 \times 10^{-3}$	$1.38 \times 10^{-3}$	$1.00 \times 10^{-2}$	1.01
Median	$1.06 \times 10^{-3}$	$8.50 \times 10^{-4}$	$6.30 \times 10^{-3}$	$6.32 \times 10^{-1}$
Mode	$4.40 \times 10^{-4}$	$3.60 \times 10^{-4}$	$2.66 \times 10^{-3}$	$2.65 \times 10^{-1}$
Range	$5.25 \times 10^{-3}$	$4.63 \times 10^{-3}$	$3.37 \times 10^{-2}$	3.46
Std. Dev.	$1.40 \times 10^{-3}$	$1.25 \times 10^{-3}$	$9.07 \times 10^{-3}$	$9.24 \times 10^{-1}$
25th %ile	$6.70 \times 10^{-4}$	$5.30 \times 10^{-4}$	$3.91 \times 10^{-3}$	$3.91 \times 10^{-1}$
50th %ile	$1.06 \times 10^{-3}$	$8.50 \times 10^{-4}$	$6.30 \times 10^{-3}$	$6.32 \times 10^{-1}$
75th %ile	$1.82 \times 10^{-3}$	$1.56 \times 10^{-3}$	$1.13 \times 10^{-2}$	1.14
IQR	$1.15 \times 10^{-3}$	$1.02 \times 10^{-3}$	$7.42 \times 10^{-3}$	$7.46 \times 10^{-1}$
Skewness	1.65	1.66	1.66	1.70
Kurtosis	1.81	1.88	1.89	2.05

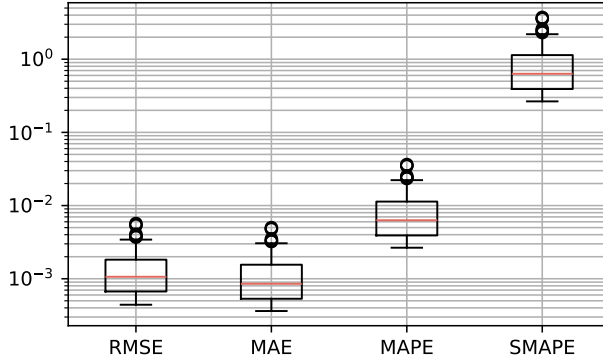


Figure 8: Results of RMSE, MAE, MAPE, and SMAPE considering 50 runs.

#### 4.7. Benchmarking

The comparative analysis presented here focuses on comparing our proposed method to other well-established DL architectures. This evaluation considers two different horizons: A short-term horizon of 5-steps ahead and a medium-term horizon of 60-steps ahead. The results of the short-term horizon are presented in Table 9, and the results of the medium-term horizon are presented in Table 8.

Table 8: Comparative analysis of DL models for a short-term horizon.

Model	RMSE	MAE	MAPE	SMAPE	Time (s)
Standard RNN	$5.41 \times 10^{-3}$	$5.09 \times 10^{-3}$	$3.87 \times 10^{-2}$	3.96	<b>3.27</b>
Dilated RNN	$3.48 \times 10^{-3}$	$3.11 \times 10^{-3}$	$2.37 \times 10^{-2}$	2.40	9.69
LSTM	$2.06 \times 10^{-3}$	$1.95 \times 10^{-3}$	$1.48 \times 10^{-2}$	1.49	3.65
GRU	$1.87 \times 10^{-3}$	$1.71 \times 10^{-3}$	$1.30 \times 10^{-2}$	1.29	4.12
TFT	$7.20 \times 10^{-4}$	$5.81 \times 10^{-4}$	$4.43 \times 10^{-3}$	$4.42 \times 10^{-1}$	$1.08 \times 10^2$
TCN	$5.87 \times 10^{-3}$	$4.85 \times 10^{-3}$	$3.69 \times 10^{-2}$	3.59	4.03
Informer	$1.22 \times 10^{-2}$	$9.33 \times 10^{-3}$	$7.09 \times 10^{-2}$	7.30	$7.88 \times 10^1$
DeepNPTS	$6.67 \times 10^{-4}$	$6.02 \times 10^{-4}$	$4.59 \times 10^{-3}$	$4.58 \times 10^{-1}$	3.34
N-BEATS	$8.97 \times 10^{-4}$	$7.48 \times 10^{-4}$	$5.71 \times 10^{-3}$	$5.69 \times 10^{-1}$	$3.36 \times 10^1$
NHITS	$8.74 \times 10^{-4}$	$7.34 \times 10^{-4}$	$5.60 \times 10^{-3}$	$5.58 \times 10^{-1}$	$4.89 \times 10^1$
Our	<b><math>2.24 \times 10^{-4}</math></b>	<b><math>1.84 \times 10^{-4}</math></b>	<b><math>1.41 \times 10^{-3}</math></b>	<b><math>1.41 \times 10^{-1}</math></b>	$1.67 \times 10^1$

Best results in bold

For a short-term horizon, the most promising results were considering the TFT and the

DeepNPTS that had an RMSE of  $7.20 \times 10^{-4}$  and  $6.67 \times 10^{-4}$  respectively. In this evaluation, the TFT needed a longer time to be computed, which is not an issue here, considering that the analysis is performed offline, and the time required for training is just for computation comparison. Our proposed model (optimized LLM) outperforms all these state-of-the-art models, having an RMSE of  $2.24 \times 10^{-4}$  for a short-term horizon.

Table 9: Comparative analysis of DL models for a medium-term horizon.

Model	RMSE	MAE	MAPE	SMAPE	Time (s)
Standard RNN	$1.42 \times 10^{-2}$	$1.34 \times 10^{-2}$	$9.77 \times 10^{-2}$	$1.03 \times 10^1$	6.07
Dilated RNN	$2.69 \times 10^{-2}$	$2.64 \times 10^{-2}$	$1.94 \times 10^{-1}$	$2.15 \times 10^1$	$1.40 \times 10^1$
LSTM	$2.19 \times 10^{-2}$	$2.11 \times 10^{-2}$	$1.54 \times 10^{-1}$	$1.68 \times 10^1$	<b>5.81</b>
GRU	$1.21 \times 10^{-2}$	$9.32 \times 10^{-3}$	$6.71 \times 10^{-2}$	7.10	$1.15 \times 10^1$
TFT	$1.97 \times 10^{-2}$	$1.68 \times 10^{-2}$	$1.23 \times 10^{-1}$	$1.13 \times 10^1$	$1.31 \times 10^3$
TCN	$3.59 \times 10^{-2}$	$3.41 \times 10^{-2}$	$2.53 \times 10^{-1}$	$2.22 \times 10^1$	5.96
Informer	$1.05 \times 10^{-1}$	$5.10 \times 10^{-2}$	$3.73 \times 10^{-1}$	$3.79 \times 10^1$	$8.02 \times 10^2$
DeepNPTS	$7.40 \times 10^{-3}$	$6.01 \times 10^{-3}$	$4.34 \times 10^{-2}$	4.48	8.81
N-BEATS	$5.22 \times 10^{-3}$	$3.73 \times 10^{-3}$	$2.68 \times 10^{-2}$	2.73	$4.00 \times 10^1$
NHITS	$6.94 \times 10^{-3}$	$4.95 \times 10^{-3}$	$3.55 \times 10^{-2}$	3.67	$5.11 \times 10^1$
Our	<b><math>1.21 \times 10^{-3}</math></b>	<b><math>9.30 \times 10^{-4}</math></b>	<b><math>6.77 \times 10^{-3}</math></b>	<b><math>6.73 \times 10^{-1}</math></b>	$1.68 \times 10^1$

Best results in bold

For a medium-term horizon (horizon = 60), as shown in Table 9, the state-of-the-art models that showed the best results were DeepNPTS, N-BEATS, and NHITS with an RMSE below than  $\times 10^{-2}$ . The algorithm proposed in this paper had better results with an RMSE of  $1.21 \times 10^{-3}$ , which clearly shows better performance in predicting future samples.

## 5. Conclusion

In this paper, a hybrid model integrating a filtering input stage and an LLM applied for time series, optimized via the Optuna framework, was proposed for insulator fault prediction. The time series of the leakage current of the insulators is based on a high-voltage experiment with artificial contamination. Considering an evaluation of CF, HP, STL, MSTL, EWT, Butterworth, and EDM filters, the EWT showed more promising results with its default setup. Therefore, the EWT decomposed time series signals, mitigating noise and non-stationary effects. These decomposed signals were subsequently forecasted by an optimized LLM, which demonstrated robust capabilities in modeling complex temporal dependencies inherent in insulator degradation patterns.

The experimental results underscore the superiority of the optimized LLM framework in comparison to the state-of-the-art DL models, achieving an RMSE equal to  $2.24 \times 10^{-4}$  for a short-term horizon (5 steps ahead) and  $1.21 \times 10^{-3}$  for a medium-term horizon (60 steps ahead) in insulator fault detection. The proposed methodology enhances the reliability of power grid maintenance and provides a generalizable framework for predictive maintenance in industrial systems.

Future work could explore the integration of real-time adaptive decomposition techniques, expand the model's interpretability for operational decision-making, and validate the framework on larger cross-domain datasets. Deploying the monitoring model on-site can promote practical implementation in smart grid applications.

## Acknowledgements

This work was partially supported by the Natural Sciences and Engineering Research Council of Canada (NSERC), funding reference number DDG-2024-00035. Cette recherche a été financée par le Conseil de recherches en sciences naturelles et en génie du Canada (CRSNG), numéro de référence DDG-2024-00035. This research was also partially funded by the Fundação para a Ciência e a Tecnologia (FCT, <https://ror.org/00snfq58>) under Grants UIDB/04111/2020, UIDB/00066/2020, UIDB/00408/2020 and the LASIGE Research Unit, ref. UID/000408/2025, as well as by the Instituto Lusófono de Investigação e Desenvolvimento (ILIND), Portugal, under Project COFAC/ILIND/COPELABS/1/2024.

## Declaration of competing interest

The authors declare that they have no known competing financial interests or personal relationships that could have appeared to influence the work reported in this paper.

## CRedit authorship contribution statement

**João Pedro Matos-Carvalho** and **Stefano Frizzo Stefenon**: Conceptualization, software, formal analysis, writing - original draft. **Valderi Reis Quietinho Leithard** and **Kin-Choong Yow**: Supervision, writing - review & editing.

## Data availability

For future analysis, the original data is available at: <https://github.com/SFStefenon/LeakageCurrent>.

## References

- [1] Mohammad Akbari and Amir Abbas Shayegani-Akmal. Experimental investigation on the accelerated aging of silicone rubber insulators based on thermal stress. *International Journal of Electrical Power & Energy Systems*, 149:109049, 2023. doi: 10.1016/j.ijepes.2023.109049.
- [2] Rafael Castillo-Sierra, Oscar Oviedo-Trespalacios, John E Candelo-Becerra, Jose D Soto, and Maria Calle. A novel method for prediction of washing cycles of electrical insulators in high pollution environments. *International Journal of Electrical Power & Energy Systems*, 130:107026, 2021. doi: 10.1016/j.ijepes.2021.107026.
- [3] Yanpeng Hao, Yingying Zhang, Zikui Shen, Lin Liu, Congwei Yao, Shenglong Huang, Zhimin Zhang, Yao Zheng, and Lin Yang. Ultrasonic longitudinal wave reflection propagation model and defect detection method for the cone of 126-kV three-phase basin insulators. *IEEE Transactions on Instrumentation and Measurement*, 73:1–8, 2024. doi: 10.1109/TIM.2024.3412189.
- [4] Xinhao Qiao, Zhijin Zhang, Raji Sundararajan, Xingliang Jiang, Jianping Hu, and Zhen Fang. The failure arc paths of the novel device combining an arrester and an insulator under different pollution levels. *International Journal of Electrical Power & Energy Systems*, 125:106549, 2021. doi: 10.1016/j.ijepes.2020.106549.



- [5] Yong Liu, Hongbao Zong, Sheng Gao, and BX Du. Contamination deposition and discharge characteristics of outdoor insulators in fog-haze conditions. *International Journal of Electrical Power & Energy Systems*, 121:106176, 2020. doi: 10.1016/j.ijepes.2020.106176.
- [6] L Cui and M Ramesh. Prediction of flashover voltage using electric field measurement on clean and polluted insulators. *International Journal of Electrical Power & Energy Systems*, 116:105574, 2020. doi: 10.1016/j.ijepes.2019.105574.
- [7] Hemant Yadav and Amit Thakkar. NOA-LSTM: An efficient LSTM cell architecture for time series forecasting. *Expert Systems with Applications*, 238:122333, 2024. doi: 10.1016/j.eswa.2023.122333.
- [8] Tiago Mota Dutra, José Carlos Dias, and João CA Teixeira. Measuring financial cycles: Empirical evidence for Germany, United Kingdom and United States of America. *International Review of Economics & Finance*, 79:599–630, 2022. doi: 10.1016/j.iref.2022.02.039.
- [9] Yves S Schüler. Filtering economic time series: On the cyclical properties of Hamilton’s regression filter and the Hodrick-Prescott filter. *Review of Economic Dynamics*, 54:101237, 2024. doi: 10.1016/j.red.2024.101237.
- [10] Houtian He, Shangce Gao, Ting Jin, Syuhei Sato, and Xingyi Zhang. A seasonal-trend decomposition-based dendritic neuron model for financial time series prediction. *Applied Soft Computing*, 108:107488, 2021. doi: 10.1016/j.asoc.2021.107488.
- [11] Kasun Bandara, Rob J Hyndman, and Christoph Bergmeir. MSTL: A seasonal-trend decomposition algorithm for time series with multiple seasonal patterns. *International Journal of Operational Research*, 52(1):79–98, 2025. doi: 10.1504/IJOR.2025.143957.
- [12] Xianshuang Yao, Huiyu Wang, Yanning Shao, Zhanjun Huang, Shengxian Cao, and Qingchuan Ma. Multi-state delayed echo state network with empirical wavelet transform for time series prediction. *Applied Intelligence*, 54(6):4646–4667, 2024. doi: 10.1007/s10489-024-05386-1.
- [13] Xueyan Hu, Wei Liu, and Hua Huo. An intelligent network traffic prediction method based on Butterworth filter and CNN-LSTM. *Computer Networks*, 240:110172, 2024. doi: 10.1016/j.comnet.2024.110172.
- [14] Anne Carolina Rodrigues Klaar, Laio Oriel Seman, Viviana Cocco Mariani, and Leandro dos Santos Coelho. Random convolutional kernel transform with empirical mode decomposition for classification of insulators from power grid. *Sensors*, 24(4):1113, 2024. doi: 10.3390/s24041113.
- [15] Stefano Frizzo Stefenon, Laio Oriel Seman, Luiza Scapinello Aquino da Silva, Viviana Cocco Mariani, and Leandro dos Santos Coelho. Hypertuned temporal fusion transformer for multi-horizon time series forecasting of dam level in hydroelectric power plants. *International Journal of Electrical Power & Energy Systems*, 157:109876, 2024. doi: 10.1016/j.ijepes.2024.109876.
- [16] PHV Rocha, EG Costa, AR Serres, GVR Xavier, JEB Peixoto, and RL Lins. Inspection in overhead insulators through the analysis of the irradiated RF spectrum. *International Journal of Electrical Power & Energy Systems*, 113:355–361, 2019. doi: 10.1016/j.ijepes.2019.05.060.

- [17] Xinyu Liu, Xiren Miao, Hao Jiang, and Jing Chen. Box-point detector: A diagnosis method for insulator faults in power lines using aerial images and convolutional neural networks. *IEEE Transactions on Power Delivery*, 36(6):3765–3773, 2021. doi: 10.1109/TPWRD.2020.3048935.
- [18] Zhanshe Yang, Zheng Xu, and Yunhao Wang. Bidirection-Fusion-YOLOv3: An improved method for insulator defect detection using UAV image. *IEEE Transactions on Instrumentation and Measurement*, 71:1–8, 2022. doi: 10.1109/TIM.2022.3201499.
- [19] Jianqi Li, Yaqian Xu, Keheng Nie, Binfang Cao, Sinuo Zuo, and Jiang Zhu. PEDNet: A lightweight detection network of power equipment in infrared image based on YOLOv4-Tiny. *IEEE Transactions on Instrumentation and Measurement*, 72:1–12, 2023. doi: 10.1109/TIM.2023.3235416.
- [20] Ming Zhou, Bo Li, Jue Wang, and Shi He. Fault detection method of glass insulator aerial image based on the improved YOLOv5. *IEEE Transactions on Instrumentation and Measurement*, 72:1–10, 2023. doi: 10.1109/TIM.2023.3269099.
- [21] Stefano Frizzo Stefenon, Laio Oriel Seman, Anne Carolina Rodrigues Klaar, Raúl García Ovejero, and Valderi Reis Quietinho Leithardt. Hypertuned-YOLO for interpretable distribution power grid fault location based on EigenCAM. *Ain Shams Engineering Journal*, 15(6):102722, 2024. doi: 10.1016/j.asej.2024.102722.
- [22] Stefano Frizzo Stefenon, Gurmail Singh, Bruno José Souza, Roberto Zanetti Freire, and Kin-Choong Yow. Optimized hybrid YOLOu-Quasi-ProtoPNet for insulators classification. *IET Generation, Transmission & Distribution*, 17(15):3501–3511, 2023. doi: 10.1049/gtd2.12886.
- [23] Fangming Deng, Zhongxin Xie, Wei Mao, Bing Li, Yun Shan, Baoquan Wei, and Han Zeng. Research on edge intelligent recognition method oriented to transmission line insulator fault detection. *International Journal of Electrical Power & Energy Systems*, 139:108054, 2022. doi: 10.1016/j.ijepes.2022.108054.
- [24] Min He, Liang Qin, Xinlan Deng, and Kaipei Liu. MFI-YOLO: Multi-fault insulator detection based on an improved YOLOv8. *IEEE Transactions on Power Delivery*, 39(1):168–179, 2024. doi: 10.1109/TPWRD.2023.3328178.
- [25] Wenqing Zhao, Minfu Xu, Xingfu Cheng, and Zhenbing Zhao. An insulator in transmission lines recognition and fault detection model based on improved faster RCNN. *IEEE Transactions on Instrumentation and Measurement*, 70:1–8, 2021. doi: 10.1109/TIM.2021.3112227.
- [26] Yu Lin, Lianfang Tian, and Qiliang Du. Automatic overheating defect diagnosis based on rotated detector for insulator in infrared image. *IEEE Sensors Journal*, 23(21):26245–26258, 2023. doi: 10.1109/JSEN.2023.3315280.
- [27] Gurmail Singh, Stefano Frizzo Stefenon, and Kin-Choong Yow. Interpretable visual transmission lines inspections using pseudo-prototypical part network. *Machine Vision and Applications*, 34(3):41, 2023. doi: 10.1007/s00138-023-01390-6.
- [28] N. F. Sopelsa Neto, S. F. Stefenon, L. H. Meyer, R. G. Ovejero, and V. R. Q. Leithardt. Fault prediction based on leakage current in contaminated insulators using enhanced time series forecasting models. *Sensors*, 22(16):6121, 2022. doi: 10.3390/s22166121.

- [29] Stefano Frizzo Stefenon, Laio Oriel Seman, Nemesio Fava Sopelsa Neto, Luiz Henrique Meyer, Viviana Cocco Mariani, and Leandro dos Santos Coelho. Group method of data handling using Christiano-Fitzgerald random walk filter for insulator fault prediction. *Sensors*, 23(13):6118, 2023. doi: 10.3390/s23136118.
- [30] Lijun Jin, Gangjie Zhou, Zhikang Yuan, Haifeng Jin, and Xiaokun Man. Study on initial discharge process of insulator pollution flashover considering quantum transition. *IEEE Transactions on Dielectrics and Electrical Insulation*, 29(5):1818–1827, 2022. doi: 10.1109/TDEI.2022.3190346.
- [31] Liping Zhang, Xiao Li, Junmei Zhao, Yewei Zhang, and Qiang Zhang. Flashover detection and anomaly prediction in aerial images of insulator strings in complex environments. *IEEE Access*, 12:94926–94935, 2024. doi: 10.1109/ACCESS.2024.3424406.
- [32] Yang Xing, Zhongxu Hu, Peng Hang, and Chen Lv. Learning from the dark side: A parallel time series modelling framework for forecasting and fault detection on intelligent vehicles. *IEEE Transactions on Intelligent Vehicles*, 9(2):3205–3219, 2024. doi: 10.1109/TIV.2023.3342648.
- [33] Jianwen Guo, Zhenpeng Lao, Ming Hou, Chuan Li, and Shaohui Zhang. Mechanical fault time series prediction by using EFMSAE-LSTM neural network. *Measurement*, 173:108566, 2021. doi: 10.1016/j.measurement.2020.108566.
- [34] Hongling Xu, Ruizhe Ma, Li Yan, and Zongmin Ma. Two-stage prediction of machinery fault trend based on deep learning for time series analysis. *Digital Signal Processing*, 117:103150, 2021. doi: 10.1016/j.dsp.2021.103150.
- [35] Haiying Liu, Ruizhe Ma, Daiyi Li, Li Yan, and Zongmin Ma. Machinery fault diagnosis based on deep learning for time series analysis and knowledge graphs. *journal of signal processing systems*, 93:1433–1455, 2021. doi: 10.1007/s11265-021-01718-3.
- [36] Chia-Yu Hsu and Wei-Chen Liu. Multiple time-series convolutional neural network for fault detection and diagnosis and empirical study in semiconductor manufacturing. *Journal of Intelligent Manufacturing*, 32(3):823–836, 2021. doi: 10.1007/s10845-020-01591-0.
- [37] Kai He, Daojie Yu, Dong Wang, Mengjuan Chai, Shuntian Lei, and Changlin Zhou. Graph attention network-based fault detection for uavs with multivariant time series flight data. *IEEE Transactions on Instrumentation and Measurement*, 71:1–13, 2022. doi: 10.1109/TIM.2022.3219489.
- [38] Yuhong Jin, Lei Hou, and Yushu Chen. A time series transformer based method for the rotating machinery fault diagnosis. *Neurocomputing*, 494:379–395, 2022. doi: 10.1016/j.neucom.2022.04.111.
- [39] Mengyu Chen, Zechen Li, Xiang Lei, Shan Liang, Shuangxin Zhao, and Yiting Su. Un-supervised fault detection driven by multivariate time series for aeroengines. *Journal of Aerospace Engineering*, 36(2):04022129, 2023. doi: 10.1061/JAEEZ.ASENG-4576.
- [40] Kai Zhang, Wangze Ning, Yudi Zhu, Zhuoheng Li, Tao Wang, Wenkai Jiang, Min Zeng, and Zhi Yang. Gaussian-linearized transformer with tranquilized time-series decomposition methods for fault diagnosis and forecasting of methane gas sensor arrays. *Applied Sciences*, 14(1):218, 2023. doi: 10.3390/app14010218.

- [41] Yuan Xie, Jisheng Zhao, Baohua Qiang, Luzhong Mi, Chenghua Tang, and Longge Li. Attention mechanism-based cnn-lstm model for wind turbine fault prediction using SSN ontology annotation. *Wireless Communications and Mobile Computing*, 2021(1):6627588, 2021. doi: 10.1155/2021/6627588.
- [42] Rajeevan Arunthavanathan, Faisal Khan, Salim Ahmed, and Syed Imtiaz. A deep learning model for process fault prognosis. *Process Safety and Environmental Protection*, 154:467–479, 2021. doi: 10.1016/j.psep.2021.08.022.
- [43] H Du Nguyen, Kim Phuc Tran, Sébastien Thomassey, and Moez Hamad. Forecasting and anomaly detection approaches using lstm and lstm autoencoder techniques with the applications in supply chain management. *International Journal of Information Management*, 57:102282, 2021. doi: 10.1016/j.ijinfomgt.2020.102282.
- [44] Xiaoyu Zhang, Liwei Tang, and Jiusheng Chen. Fault diagnosis for electro-mechanical actuators based on STL-HSTA-GRU and SM. *IEEE Transactions on Instrumentation and Measurement*, 70:1–16, 2021. doi: 10.1109/TIM.2021.3127641.
- [45] Xiangjie Huang, Xun Lang, Songhua Liu, Peng Li, Tao Guo, and Li Yu. Dilated autoformer: An improved model for predicting the state of transformer bushing. In *2024 43rd Chinese Control Conference (CCC)*, pages 8858–8863, Kunming, China, 2024. doi: 10.23919/CCC63176.2024.10662411.
- [46] Xiaohan Chen, Beike Zhang, and Dong Gao. Bearing fault diagnosis base on multi-scale cnn and lstm model. *Journal of Intelligent Manufacturing*, 32(4):971–987, 2021. doi: 10.1007/s10845-020-01600-2.
- [47] Nathielle Waldrigues Branco, Mariana Santos Matos Cavalca, Stefano Frizzo Stefenon, and Valderi Reis Quietinho Leithardt. Wavelet LSTM for fault forecasting in electrical power grids. *Sensors*, 22(21):8323, 2022. doi: 10.3390/s22218323.
- [48] A. Medeiros, A. Sartori, S. F. Stefenon, L. H. Meyer, and A. Nied. Comparison of artificial intelligence techniques to failure prediction in contaminated insulators based on leakage current. *Journal of Intelligent & Fuzzy Systems*, 42(4):3285–3298, 2022. doi: 10.3233/JIFS-211126.
- [49] Laio Oriel Seman, Stefano Frizzo Stefenon, Viviana Cocco Mariani, and Leandro Santos Coelho. Ensemble learning methods using the Hodrick–Prescott filter for fault forecasting in insulators of the electrical power grids. *International Journal of Electrical Power & Energy Systems*, 152:109269, 2023. ISSN 0142-0615. doi: 10.1016/j.ijepes.2023.109269.
- [50] Anne Carolina Rodrigues Klaar, Stefano Frizzo Stefenon, Laio Oriel Seman, Viviana Cocco Mariani, and Leandro Santos Coelho. Optimized EWT-Seq2Seq-LSTM with attention mechanism to insulators fault prediction. *Sensors*, 23(6):3202, 2023. doi: 10.3390/s23063202.
- [51] S. F. Stefenon, M. H. D. M. Ribeiro, A. Nied, V. C. Mariani, L. S. Coelho, V. R. Q. Leithardt, L. A. Silva, and L. O. Seman. Hybrid wavelet stacking ensemble model for insulators contamination forecasting. *IEEE Access*, 9:66387–66397, 2021. doi: 10.1109/ACCESS.2021.3076410.

- [52] Nathielle Waldrigues Branco, Mariana Santos Matos Cavalca, and Raúl García Ovejero. Bootstrap aggregation with christiano–fitzgerald random walk filter for fault prediction in power systems. *Electrical Engineering*, 106(3):3657–3670, 2024. doi: 10.1007/s00202-023-02146-1.
- [53] Stéfano Frizzo Stefenon, Roberto Zanetti Freire, Leandro Santos Coelho, Luiz Henrique Meyer, Rafael Bartnik Grebogi, William Gouvêa Buratto, and Ademir Nied. Electrical insulator fault forecasting based on a wavelet neuro-fuzzy system. *Energies*, 13(2):484, 2020. doi: 10.3390/en13020484.
- [54] Hansika Hewamalage, Christoph Bergmeir, and Kasun Bandara. Recurrent neural networks for time series forecasting: Current status and future directions. *International Journal of Forecasting*, 37(1):388–427, 2021. ISSN 0169-2070. doi: 10.1016/j.ijforecast.2020.06.008.
- [55] Junlong Tong, Liping Xie, Wankou Yang, Kanjian Zhang, and Junsheng Zhao. Enhancing time series forecasting: A hierarchical transformer with probabilistic decomposition representation. *Information Sciences*, 647:119410, 2023. ISSN 0020-0255. doi: 10.1016/j.ins.2023.119410.
- [56] Bryan Lim, Sercan O. Arik, Nicolas Loeff, and Tomas Pfister. Temporal fusion transformers for interpretable multi-horizon time series forecasting. *International Journal of Forecasting*, 37(4):1748–1764, 2021. ISSN 0169-2070. doi: 10.1016/j.ijforecast.2021.03.012.
- [57] Boris N. Oreshkin, Dmitri Carpov, Nicolas Chapados, and Yoshua Bengio. N-BEATS: Neural basis expansion analysis for interpretable time series forecasting. In *International Conference on Learning Representations*, pages 1–31, Addis Ababa, Ethiopia, 2020. ICLR.
- [58] Yitian Chen, Yanfei Kang, Yixiong Chen, and Zizhuo Wang. Probabilistic forecasting with temporal convolutional neural network. *Neurocomputing*, 399:491–501, 2020. ISSN 0925-2312. doi: 10.1016/j.neucom.2020.03.011.
- [59] Guolin Ke, Qi Meng, Thomas Finley, Taifeng Wang, Wei Chen, Weidong Ma, Qiwei Ye, and Tie-Yan Liu. LightGBM: A highly efficient gradient boosting decision tree. In *Conference on Neural Information Processing Systems*, volume 31, pages 1–9, Long Beach, USA, 2017. NIPS.
- [60] David Salinas, Valentin Flunkert, Jan Gasthaus, and Tim Januschowski. Deepar: Probabilistic forecasting with autoregressive recurrent networks. *International Journal of Forecasting*, 36(3):1181–1191, 2020. ISSN 0169-2070. doi: 10.1016/j.ijforecast.2019.07.001.
- [61] Zonghan Wu, Shirui Pan, Guodong Long, Jing Jiang, Xiaojun Chang, and Chengqi Zhang. Connecting the dots: Multivariate time series forecasting with graph neural networks. In *International Conference on Knowledge Discovery & Data Mining*, volume 26, page 753–763, New York, USA, 2020. ACM. doi: 10.1145/3394486.3403118.
- [62] Bing Yu, Haoteng Yin, and Zhanxing Zhu. Spatio-temporal graph convolutional networks: A deep learning framework for traffic forecasting. In *International Joint Conference on Artificial Intelligence*, volume 27, pages 3634–3640, Stockholm, Sweden, 2018. IJCAI. doi: 10.24963/ijcai.2018/505.

- [63] Jianqin Zheng, Jian Du, Bohong Wang, Jiří Jaromír Klemeš, Qi Liao, and Yongtu Liang. A hybrid framework for forecasting power generation of multiple renewable energy sources. *Renewable and Sustainable Energy Reviews*, 172:113046, 2023. ISSN 1364-0321. doi: 10.1016/j.rser.2022.113046.
- [64] Hossein Abbasian Mohammadi, Sedigheh Ghofrani, and Ali Nikseresht. Using empirical wavelet transform and high-order fuzzy cognitive maps for time series forecasting. *Applied Soft Computing*, 135:109990, 2023. ISSN 1568-4946. doi: 10.1016/j.asoc.2023.109990.
- [65] Ming Jin, Shiyu Wang, Lintao Ma, Zhixuan Chu, James Y. Zhang, Xiaoming Shi, Pin-Yu Chen, Yuxuan Liang, Yuan-Fang Li, Shirui Pan, and Qingsong Wen. Time-LLM: Time series forecasting by reprogramming large language models. In *International Conference on Learning Representations*, volume 12, pages 1–24, Vienna, Austria, 2024. ICLR.
- [66] Shahram Hanifi, Andrea Cammarono, and Hossein Zare-Behtash. Advanced hyperparameter optimization of deep learning models for wind power prediction. *Renewable Energy*, 221:119700, 2024. ISSN 0960-1481. doi: 10.1016/j.renene.2023.119700.
- [67] Polipireddy Srinivas and Rahul Katarya. hyOPTXg: OPTUNA hyper-parameter optimization framework for predicting cardiovascular disease using XGBoost. *Biomedical Signal Processing and Control*, 73:103456, 2022. doi: 10.1016/j.bspc.2021.103456.
- [68] Zuokun Ouyang, Philippe Ravier, and Meryem Jabloun. STL decomposition of time series can benefit forecasting done by statistical methods but not by machine learning ones. *Engineering Proceedings*, 5(1):42, 2021. doi: 10.3390/engproc2021005042.
- [69] Debesh Bhowmik, Sandeep Poddar, et al. Cyclical and seasonal patterns of india’s gdp growth rate through the eyes of hamilton and hodrick prescott filter models. *Advancement in Management and Technology (AMT)*, 1(3):7–17, 2021. doi: 10.46977/apjmt.2021v01i03.002.
- [70] Ziqiang Li, Yun Liu, and Gouhei Tanaka. Multi-reservoir echo state networks with hodrick–prescott filter for nonlinear time-series prediction. *Applied Soft Computing*, 135:110021, 2023. doi: 10.1016/j.asoc.2023.110021.
- [71] Neslihan Sakarya and Robert M de Jong. The spectral analysis of the hodrick–prescott filter. *Journal of Time Series Analysis*, 43(3):479–489, 2022. doi: 10.1111/jtsa.12622.
- [72] Li Xu, Yanxia Ou, Jingjing Cai, Jin Wang, Yang Fu, and Xiaoyan Bian. Offshore wind speed assessment with statistical and attention-based neural network methods based on stl decomposition. *Renewable Energy*, 216:119097, 2023. doi: 10.1016/j.renene.2023.119097.
- [73] Anne Carolina Rodrigues Klaar, Stefano Frizzo Stefenon, Laio Oriel Seman, Viviana Cocco Mariani, and Leandro Santos Coelho. Structure optimization of ensemble learning methods and seasonal decomposition approaches to energy price forecasting in Latin America: A case study about Mexico. *Energies*, 16(7):3184, 2023. doi: 10.3390/en16073184.
- [74] Amirhossein Sohrabbeig, Omid Ardakanian, and Petr Musilek. Decompose and conquer: Time series forecasting with multiseasonal trend decomposition using loess. *Forecasting*, 5(4):684–696, 2023. doi: 10.3390/forecast5040037.
- [75] Manel Rhif, Ali Ben Abbes, Beatriz Martinez, Rogier de Jong, Yanfang Sang, and Imed Riadh Farah. Detection of trend and seasonal changes in non-stationary remote sensing data:

- Case study of tunisia vegetation dynamics. *Ecological Informatics*, 69:101596, 2022. doi: 10.1016/j.ecoinf.2022.101596.
- [76] Mohammed Elseidi. MSTL-NNAR: A new hybrid model of machine learning and time series decomposition for wind speed forecasting. *Stochastic Environmental Research and Risk Assessment*, 38:2613–2632, 2024. doi: 10.1007/s00477-024-02701-7.
- [77] Hossein Abbasian Mohammadi, Sedigheh Ghofrani, and Ali Nikseresht. Using empirical wavelet transform and high-order fuzzy cognitive maps for time series forecasting. *Applied Soft Computing*, 135:109990, 2023. doi: 10.1016/j.asoc.2023.109990.
- [78] Lu Peng, Lin Wang, De Xia, and Qinglu Gao. Effective energy consumption forecasting using empirical wavelet transform and long short-term memory. *Energy*, 238:121756, 2022. doi: 10.1016/j.energy.2021.121756.
- [79] Wei Liu and Wei Chen. Recent advancements in empirical wavelet transform and its applications. *IEEE Access*, 7:103770–103780, 2019. doi: 10.1109/ACCESS.2019.2930529.
- [80] Shibendu Mahata, Norbert Herencsar, and David Kubanek. Optimal approximation of fractional-order butterworth filter based on weighted sum of classical butterworth filters. *IEEE Access*, 9:81097–81114, 2021. doi: 10.1109/ACCESS.2021.3085515.
- [81] Pushpendra Singh, Amit Singhal, Binish Fatimah, and Anubha Gupta. A novel PRFB decomposition for non-stationary time-series and image analysis. *Signal Processing*, 207:108961, 2023. doi: 10.1016/j.sigpro.2023.108961.
- [82] Qin Guodong and Chen Zhongxian. A comparison of ocean wave height forecasting methods for ocean wave energy conversion systems. *Water*, 15(18):3256, 2023. doi: 10.3390/w15183256.
- [83] Rathachai Chawuthai, Nachaphat Ainthong, Surasee Intarawart, Niracha Boonyanaet, and Agachai Sumalee. Travel time prediction on long-distance road segments in thailand. *Applied Sciences*, 12(11):5681, 2022. doi: 10.3390/app12115681.
- [84] Wanming Ying, Jinde Zheng, Haiyang Pan, and Qingyun Liu. Permutation entropy-based improved uniform phase empirical mode decomposition for mechanical fault diagnosis. *Digital Signal Processing*, 117:103167, 2021. doi: 10.1016/j.dsp.2021.103167.
- [85] Ming-De Liu, Lin Ding, and Yu-Long Bai. Application of hybrid model based on empirical mode decomposition, novel recurrent neural networks and the arima to wind speed prediction. *Energy Conversion and Management*, 233:113917, 2021. doi: 10.1016/j.enconman.2021.113917.
- [86] Shamsu Abdullahi, Kamaluddeen Usman Danyaro, Abubakar Zakari, Izzatdin Abdul Aziz, Noor Amila Wan Abdullah Zawawi, and Shamsuddeen Adamu. Time-series large language models: A systematic review of state-of-the-art. *IEEE Access*, pages 1–28, 2025. doi: 10.1109/ACCESS.2025.3535782.
- [87] Yongqian Sun, Yang Guo, Minghan Liang, Xidao Wen, Junhua Kuang, Shenglin Zhang, Hongbo Li, Kaixu Xia, and Dan Pei. Multivariate time series anomaly detection based on pre-trained models with dual-attention mechanism. In *International Symposium on Software Reliability Engineering Workshops (ISSREW)*, volume 35, pages 73–78, Tsukuba, Japan, 2024. IEEE. doi: 10.1109/ISSREW63542.2024.00050.

- [88] Ming Jin, Shiyu Wang, Lintao Ma, Zhixuan Chu, James Y Zhang, Xiaoming Shi, Pin-Yu Chen, Yuxuan Liang, Yuan-Fang Li, Shirui Pan, et al. Time-llm: Time series forecasting by reprogramming large language models. *arXiv:2310.01728*, 2:1–24, 2024. doi: 10.48550/arXiv.2310.01728.
- [89] Georgios Samaras, Marinela Mertiri, Maria-Evgenia Xezonaki, Vasileios Theodorou, Pan-teleimon Konstantinos Chartsias, and Theodoros Bozios. Unlocking the path towards AI-native networks with optimized lightweight large language models. In *International Mediterranean Conference on Communications and Networking (MeditCom)*, volume 1, pages 108–113, Madrid, Spain, 2024. IEEE. doi: 10.1109/MeditCom61057.2024.10621076.
- [90] Zeyu Zhang, Xiaoqian Liu, Xiling Zhang, Zhishan Yang, and Jian Yao. Carbon price forecasting using optimized sliding window empirical wavelet transform and gated recurrent unit network to mitigate data leakage. *Energies*, 17(17):4358, 2024. doi: 10.3390/en17174358.
- [91] Stefano Frizzo Stefenon, Laio Oriel Seman, Evandro Cardozo da Silva, Erlon Cristian Finardi, Leandro dos Santos Coelho, and Viviana Cocco Mariani. Hypertuned wavelet convolutional neural network with long short-term memory for time series forecasting in hydroelectric power plants. *Energy*, 313:133918, 2024. ISSN 0360-5442. doi: 10.1016/j.energy.2024.133918.
- [92] Bernardo Luis Tuleski, Cristina Keiko Yamaguchi, Stefano Frizzo Stefenon, Leandro dos Santos Coelho, and Viviana Cocco Mariani. Audio-based engine fault diagnosis with wavelet, Markov blanket, ROCKET, and optimized machine learning classifiers. *Sensors (Basel, Switzerland)*, 24(22):7316, 2024. doi: 10.3390/s24227316.
- [93] Evandro Cardozo da Silva, Erlon Cristian Finardi, and Stefano Frizzo Stefenon. Enhancing hydroelectric inflow prediction in the Brazilian power system: A comparative analysis of machine learning models and hyperparameter optimization for decision support. *Electric Power Systems Research*, 230:110275, 2024. doi: 10.1016/j.epsr.2024.110275.
- [94] Adolphus Lye, Alice Cicirello, and Edoardo Patelli. Sampling methods for solving bayesian model updating problems: A tutorial. *Mechanical Systems and Signal Processing*, 159: 107760, 2021. doi: 10.1016/j.ymsp.2021.107760.
- [95] IEC 60507. Artificial pollution tests on high-voltage ceramic and glass insulators to be used on A.C. systems. International standard, International Electrotechnical Commission (IEC), Geneva, Switzerland, March 2013.